

The cosmic star formation rate evolution from $z = 5$ to $z = 0$ from the VIMOS VLT deep survey[★]

L. Tresse¹, O. Ilbert^{1,2}, E. Zucca³, G. Zamorani³, S. Bardelli³, S. Arnouts¹, S. Paltani^{4,5}, L. Pozzetti³, D. Bottini⁶, B. Garilli⁶, V. Le Brun¹, O. Le Fèvre¹, D. Maccagni⁶, J.-P. Picat⁷, R. Scaramella^{8,9}, M. Scodreggio⁶, G. Vettolani⁸, A. Zanichelli⁸, C. Adami¹, M. Arnaboldi⁹, M. Bolzonella³, A. Cappi³, S. Charlot¹⁰, P. Ciliegi³, T. Contini⁷, S. Foucaud¹¹, P. Franzetti⁶, I. Gavignaud¹², L. Guzzo¹³, A. Iovino¹³, H. J. McCracken^{10,14}, B. Marano¹⁵, C. Marinoni^{1,16}, A. Mazure¹, B. Meneux^{6,13}, R. Merighi³, R. Pellò⁷, A. Pollo^{1,17}, M. Radovich⁹, M. Bondi⁸, A. Bongiorno¹⁵, G. Busarello⁹, O. Cucciati^{13,17}, F. Lamareille⁷, G. Mathez⁷, Y. Mellier^{10,14}, P. Merluzzi⁹, and V. Ripepi⁹

(Affiliations can be found after the references)

Received 31 August 2006 / Accepted 26 April 2007

ABSTRACT

Context. The VIMOS VLT Deep Survey (VVDS) was undertaken to map the evolution of galaxies, large scale structures, and active galaxy nuclei from the redshift spectroscopic measurements of $\sim 10^5$ objects down to an apparent magnitude $I_{AB} = 24$, in combination with a multi-wavelength acquisition for radio, infrared, optical, ultraviolet, and X-rays data.

Aims. We present the evolution of the comoving star formation rate (SFR) density in the redshift range $0 < z < 5$ using the first epoch data release of the VVDS, that is 11564 spectra over 2200 arcmin² in two fields of view, the VVDS-0226-04 and the VVDS-CDFS-0332-27, and the cosmological parameters $(\Omega_M, \Omega_\Lambda, h) = (0.3, 0.7, 0.7)$.

Methods. We study the multi-wavelength non dust-corrected luminosity densities at $0 < z < 2$ from the rest-frame far ultraviolet to the optical passbands, and the rest-frame 1500 Å luminosity functions and densities at $2.7 < z < 5$.

Results. They evolve from $z = 1.2$ to $z = 0.05$ according to $(1+z)^x$ with $x = 2.05, 1.94, 1.92, 1.14, 0.73, 0.42$, and 0.30 in the FUV-1500, NUV-2800, U -3600, B -4400, V -5500, R -6500, and I -7900 passbands, respectively. From $z = 1.2$ to $z = 0.2$ the B -band density for the irregular-like galaxies decreases markedly by a factor 3.5 while it increases by a factor 1.7 for the elliptical-like galaxies. We identify several SFR periods; from $z = 5$ to 3.4 the FUV-band density increases by at most 0.5 dex, from $z = 3.4$ to 1.2 it decreases by 0.08 dex, from $z = 1.2$ to $z = 0.05$ it declines steadily by 0.6 dex. For the most luminous $M_{AB}(1500 \text{ Å}) < -21$ galaxies the FUV-band density drops by 2 dex from $z = 3.9$ to $z = 1.2$, and for the intermediate $-21 < M_{AB}(1500 \text{ Å}) < -20$ galaxies it drops by 2 dex from $z = 0.2$ to $z = 0$. Comparing with dust corrected surveys, at $0.4 \lesssim z \lesssim 2$ the FUV seems obscured by a constant factor of ~ 1.8 –2 mag, while at $z < 0.5$ it seems progressively less obscured by up to ~ 0.9 –1 mag when the dust-deficient early-type population is increasingly dominating the B -band density.

Conclusions. The VVDS results agree with a downsizing picture where the most luminous sources cease to efficiently produce new stars 12 Gyrs ago (at $z \simeq 4$), while intermediate luminosity sources keep producing stars until 2.5 Gyrs ago (at $z \simeq 0.2$). A modest contribution of dry mergers and morphologies evolving towards early-type galaxies might contribute to increase the number density of the bright early types at $z < 1.5$. Our observed SFR density is not in agreement with a continuous smooth decrease since $z \sim 4$.

Key words. cosmology: observations – galaxies: evolution – galaxies: luminosity function, mass function

1. Introduction

1.1. The global star-formation history one decade ago

The history of the comoving space density of the star formation rate (SFR) is a key study which has undergone a spectacular explosion of publications since the pioneer work of Madau et al. (1996) in which galaxy surveys were used for the first time. Madau et al. (1996) derived the global star formation as a function of redshift combining emissivities from three distinct surveys: the $H\alpha$ -selected UCM survey (Gallego et al. 1995) at $z < 0.05$, the largest spectroscopic sample at that time, the I -band

selected Canada-France Redshift Survey at $0.2 < z < 1$ (CFRS; Lilly et al. 1996), and their own galaxy sample at $2 < z < 4.5$ using the Lyman continuum break colour-selection technique (Steidel et al. 1996) applied on the deep optical imaging, the Hubble Deep Field (HDF) survey. Nevertheless high- z sources were lower limits, and incompleteness corrections and uniform limiting magnitude were required.

The SFR density is usually derived from the mean luminosity density, or emissivity, that is $\mathcal{L} = \int_0^\infty \phi(L)LdL$. At first sight the SFR density appears a simple and useful tool to trace back the evolution of star formation and to link it with the evolution of stellar mass, but a large spread between different measurements have led to controversy. Uncertainties in conversion factors from luminosity to SFR, and in the amount of dust obscured SFR, coupled with the different selection criteria of each survey and with the uncertainty about the shape of the luminosity function, meant that the SFR history of the Universe was

[★] Based on observations collected at the European Southern Observatory Very Large Telescope, Paranal, Chile, program 070.A-9007(A), and on data obtained at the Canada-France-Hawaii Telescope, operated by the Institut National des Sciences de l'Univers of the Centre National de la Recherche Scientifique of France, the National Research Council of Canada, and the University of Hawaii.

poorly determined, and thus hotly debated. In the mid-90's the main questions that arose were: is there a peak of the cosmic star-formation history at $1.3 < z < 2.7$? By how much does interstellar dust attenuate the ionizing flux? Is the evolution so rapid below $z = 1$? Is the high-redshift dropout population representative? Does the red galaxy population evolve passively or not?

1.2. A wealth of multi-wavelength studies

Measuring the cosmic star-formation history has advanced rapidly in the last decade meanwhile one had to translate results using the standard cold dark matter (CDM) into the Λ CDM cosmology. It adds uncertainties since the cosmological constant introduces a redshift dependence to the luminosity function unless one can take back all the data needed to compute the luminosity function. Still the inferred larger distances and volumes result in decreasing luminosities and densities, and thus in a shallower SFR evolution.

On the one hand, a wealth of multi-wavelength emissivities (far- and near-ultraviolet, far- and near-infrared, radio, $H\alpha$, etc.) has been obtained, all of them being more or less directly proportional to the ionizing ultraviolet stellar spectra at $\lambda < 912 \text{ \AA}$ mainly produced by massive, young, short-lived stars (OB stars, $t < \text{few} \times 10^6 \text{ yr}$). On the other hand, supernovae events and their by-products (neutrinos and gamma rays) are proportional to the star-death rate and are also used to probe the SFR. Nevertheless these results depend most strongly on stars more massive than 3 solar mass, and require extrapolation of the initial mass function (IMF) to lower masses to obtain the SFR for all masses. Furthermore, the ultimate desired value is the amount of the interstellar gas mass transformed into stars, and the correlated gas mass return into the interstellar medium as stars deplete their initial fuel sources; it requires assumptions and models for stellar atmospheres and stellar evolution tracks.

An example of an extensive compilation drawn from the literature of SFR density measurements at $0 < z < 6$ was done by Hopkins (2004), and Hopkins & Beacom (2006), and it led to a cosmic SFR history constrained to within factors of about ~ 3 . There is now growing evidence that the evolution has no peak at $z \sim 1.5$, however it is still unclear whether at $z > 3$ the evolution flattens, or declines or continues to increase. Those remaining uncertainties show the necessity to further investigate galaxy redshift surveys to constrain galaxy assemblies. In particular, one needs to explore multi-wavelength datasets over the same field of view, and to obtain homogeneous datasets over a large redshift range.

A detailed picture of the SFR history is emerging with the advent of large, deep redshift surveys, coupled with multi-wavelength ground and space observations over the *same* sky area. These new multi-wavelength surveys are providing a better understanding of the nature and the evolution of the galaxy population (i.e., e.g. Bell et al. 2004, and references within). Indeed on one hand, one can probe the same galaxy population at different wavelengths which gives insights about stellar masses (near-infrared) and star formation (far-ultraviolet, far-infrared), possibly coupled with spectroscopic indexes. On the other hand, one can measure reliable comoving volumes with accurate redshifts and intrinsic luminosities of objects which both are key measurements to estimate luminosity functions. Furthermore observing in various windows of the electromagnetic spectrum enable to select the largest galaxy sample which includes sources with specific energy distributions, and detectable at only some

wavelengths. The accuracy in the measurement of the shape of the luminosity function, coupled with the stellar mass-to-light ratio of galaxies, is crucial to estimate the amount of baryons in stars at a given epoch of the Universe.

1.3. The detailed study of the VVDS

The Visible Multi-Object Spectrograph (VIMOS) installed on the European Southern Observatory (ESO) Very Large Telescope (VLT) was built to produce systematic large redshift surveys thanks to its high multiplex capabilities, e.g. $\sim 550 R \simeq 230$ spectra of sources observed simultaneously over 218 arcmin^2 (Le Fèvre et al. 2003). We conducted the VIMOS VLT Deep Survey (VVDS), a major multi-wavelength spectroscopic survey, to investigate the evolution of galaxies, Active Galaxy Nuclei (AGN), and large-scale structures¹.

Here we detail our work in using the *I*-selected VVDS first epoch data described in Le Fèvre et al. (2005a) to study the evolution of the luminosity density within the redshift range $0 < z < 5$. It is part of a series of papers which analyse different aspects related to the luminosity function evolution with this data set. Ilbert et al. (2005) describe the global optical luminosity functions over $0 < z < 2$. Zucca et al. (2006) explore the color-type luminosity functions over $0 < z < 1.5$. Ilbert et al. (2006a) investigate the contribution of different morphological types to the luminosity functions. Ilbert et al. (2006b) analyse the luminosity functions in different environments over $0 < z < 1.5$. Paltani et al. (2007) analyse in detail the 1700 \AA luminosity function at $3 < z < 4$. Arnouts et al. (2005) describe the 1500 \AA luminosity functions over $0 < z < 1.3$ using GALEX-VVDS data. The infrared luminosity functions with K-band data and with SWIRE-VVDS data, and the luminosity functions for different spectroscopic-based classes are in preparation.

This paper is organized as follows. In Sect. 2 we present the data. In Sect. 3 we detail the methods used to estimate the comoving luminosity densities and associated uncertainties. In Sect. 4 we present the multi-wavelength global luminosity densities at $0 < z < 2$ derived in the *UBVRI* and in the near-UV, far-UV passbands. In Sect. 5 we compare our results to other surveys at $z < 2$. In Sect. 6 we investigate the luminosity densities for different galaxy types at $z < 2$. In Sect. 7 we measure the rest-frame 1500 \AA luminosity functions and densities at $2.7 < z < 5$ and we compare our results to other surveys. In Sect. 8 we detail the evolution of the global far-UV luminosity density all the way from $z = 5$ to $z = 0$, and we analyse its dependency to the luminosity. In Sect. 9 we derive the history of the star formation rate density since $z = 5$ and discuss the issue of dust obscuration. Finally in Section 10 we recap our conclusions about the evolution of the rest-frame luminosity densities in a well controlled and homogeneous *I*-selected population over the large redshift range $0 < z < 5$ as observed by the VVDS. Throughout this paper we use the AB flux normalization (Oke 1974). We adopt the set $(\Omega_M, \Omega_\Lambda, h) = (0.3, 0.7, 0.7)$ for the cosmological parameters.

2. Data

Our studied sample is taken from the *I*-band selected spectroscopic data of the first epoch observations obtained in two fields of view, VVDS-0226-04 and VVDS-CDFS (i.e. VVDS-0332-27 in the Chandra Deep Field-South) and described in

¹ <http://www.oamp.fr/virmos/>

Le Fèvre et al. (2005a) and Le Fèvre et al. (2004b). It consists of 11564 spectra and it covers 2200 arcmin² of sky area observed in five optical passbands U , B , V , R , and I (Le Fèvre et al. 2004a). In this paper we consider the well-defined selection function of the spectroscopic targets selected from the VVDS photometric parent catalogue with apparent magnitudes in the range $17.50 \leq I_{AB} \leq 24.0$. We do not use any serendipitous sources observed randomly in the slit other than the target. Spectroscopic observations were efficiently targeted using the VMMPs tool developed by our team for the spectrograph VIMOS-VLT/ESO (see Bottini et al. 2005, for details). We used the red grism (5500 to 9500 Å) and a resolution of $R = 227$. No pre-selection has been applied in terms of colors, sizes, photometric redshifts, or peculiar sources. The VVDS is based on the sole criterion of a I_{AB} flux limit.

Spectroscopic observations have been automatically processed using the VIPGI tool that we developed (Scodreggio et al. 2006) and spectroscopic determination is described in Le Fèvre et al. (2005a). The 1σ accuracy of the redshift measurements is estimated at 0.0009 from repeated VVDS observations. We emphasize that we have obtained an excellent efficiency for determining redshifts at $z < 2$ and at $z > 2.7$. At $2 < z < 2.7$ reliable spectral features are difficult to detect, and thus the efficiency to measure a redshift in this range is very poor. Observations extending further to the blue or into the near-IR are required to fill in this gap with more redshifts. We therefore present our measurements in the redshift ranges [0.05–2] and [2.7–5]. In total our targets have been classified as 7840 galaxies, 751 stars, and 71 quasars with a reliable spectroscopic identification at a confidence level higher than 81 percent (corresponding to the VVDS quality flags 2, 3, 4, and 9), 1580 spectra with an uncertain spectroscopic identification at a confidence level within [48–58] percent (corresponding to the VVDS quality flags 1) and 792 spectra not identified (corresponding to the VVDS quality flags 0). There are 7631 (1182), 31 (47) and 178 (271) reliable (uncertain) galaxy redshifts at $0 < z < 2$, $2 < z < 2.7$, and $2.7 < z < 5$ respectively. In our study, we exclude the quasars, which are easily identified thanks to the presence of large broad spectroscopic emission lines. Under the term “galaxies” we note that we include any narrow emission line AGN.

As we do not have a measured redshift for every source to a fixed magnitude limit in the observed field of view, we introduced a statistical weight, which is a function of apparent magnitude and redshift and corrects for sources not observed (*Target Sampling Rate*; TSR) and for sources for which the spectroscopic identification failed or is uncertain (*Spectroscopic Success Rate*; SSR). This statistical weight has been applied to each measured galaxy at $0 < z < 2$ as described in Ilbert et al. (2005). The SSR was estimated in two ways; using the photometric redshifts, and using the uncertain redshifts with a confidence level within [48–58] percent and assuming that the failed identifications have the same redshift distribution. The two SSR estimates were discrepant in the redshift bin $1.5 < z < 2$ only, with the former being twice as large as the latter. Using the deeper multi-wavelength observations of the Canada-France-Hawaii Legacy Survey² over the VVDS-0226 field, Ilbert et al. (2006c) obtained better photometric redshifts than in Ilbert et al. (2005). And thus we have refined our SSR estimations. In the redshift bin $1.4 < z < 2$ the SSR is changed by a multiplicative factor of 0.50, otherwise the SSR estimations did not change within the redshift range $0 < z < 1.4$ with respect to those presented in Ilbert et al. (2005).

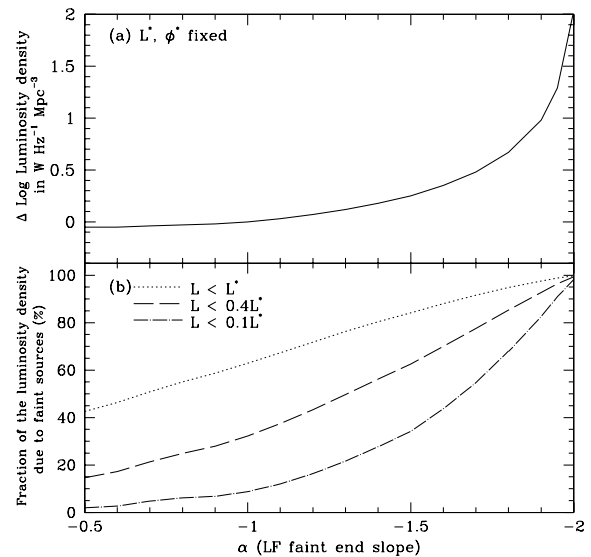


Fig. 1. a) Quantitative change in log of the comoving luminosity density, \mathcal{L} , as a function of the faint-end slope, α , of the LF for fixed L^* and ϕ^* values, compared to $\text{Log } \mathcal{L}$ for $\alpha = -1$. **b)** Fraction of \mathcal{L} as a function of α due to sources fainter than L^* (dotted line), $0.4L^*$ (dashed line), and $0.1L^*$ (dot-dashed line).

Absolute magnitude measurements are optimized accounting for the full information given by the multi-band photometric data in a way which minimizes the dependency on the templates used to fit the observed colors (see Fig. A.1 in Ilbert et al. 2005). That is, we automatically choose the observed apparent magnitude which is as close as possible to the rest-frame band redshifted in the observer frame, so the dependency to the template is null or the smallest possible. We use the templates generated with the galaxy evolution model PEGASE.2 (Fioc & Rocca-Volmerange 1997). Finally, we use a sample of galaxies which are equally visible, that is within a given absolute magnitude range which depends on the rest-frame wavelength as we describe in the next section.

3. Measuring comoving luminosity densities

3.1. Definition

Comoving luminosity densities, $\mathcal{L} = \int_0^\infty \phi(L)LdL$, depend on the shape of the luminosity function, $\phi(L)dL$. In our present study, the galaxy luminosity function (LF) follows a Schechter (1976) function characterized by a luminosity, L^* , a faint-end slope, α , and a normalization density parameter, ϕ^* , and thus $\mathcal{L} = \phi^* L^* \Gamma(\alpha + 2)$. The LF is a fundamental measurement of the statistical properties of the population of galaxies; it is the distribution of the comoving number density of galaxies as a function of their intrinsic luminosity at a given epoch. Despite its simple definition, its estimation requires careful analyses of the survey strategy, the selection criteria, and the completeness.

The faint-end slope is often measured in the range $-1 < \alpha < -2$; thus for a non-diverging density of galaxies, the LF must have a cut-off at faint luminosities. Such a cut-off has not yet been observed. This implies a high-space density of low-luminosity galaxies, but although these galaxies are very numerous, they contribute little to the mean luminosity density; for instance, sources fainter than $0.1L^*$ contribute less than 20 percent to \mathcal{L} for $\alpha < -1.3$ (see Fig. 1). As we do not observe the faintest galaxies, we use the Schechter functional form for the STY estimate (Sandage et al. 1979) to suppose the behavior of

² <http://www.cfht.hawaii.edu/Science/CFHLS/>

the LF at low luminosities. As the three Schechter parameters are highly correlated, it is necessary to build the luminosity function over the largest possible range of luminosities. Indeed, a weak constraint of the slope may have a strong impact on the determination of L^* , which is directly translated into the luminosity density estimation. Nevertheless, the latter is more robust than the estimation of each single parameter of the Schechter function alone.

3.2. Method

We estimated the LF parameters, α , M^* (or L^*), and ϕ^* , using the Algorithm for Luminosity Functions (ALF) developed within the VVDS consortium. ALF uses the non-parametric V_{\max} , SWML and C^+ and the parametric STY luminosity function estimators (see Appendixes in Ilbert et al. 2005, and references within). Each estimator presents advantages and drawbacks, and each one is affected differently by different visibility limits for the various galaxy types detected in deep flux-limited surveys. Galaxies are not equally visible in the same absolute magnitude range mainly due to the spectral type dependency on the k corrections. The bias was quantified in Ilbert et al. (2004); it affects the faint-end slope of the global LF which can be over/underestimated depending on the adopted estimator. When the differences between the estimators are larger than the statistical uncertainties, it indicates the presence of a significant bias. Thus in a given redshift range our LF parameters are estimated with data restricted to the absolute magnitude range in which all galaxy types are visible. It enables us to calculate an unbiased LF slope.

We apply two approaches to derive the luminosity density from the LF. First, we derive *minimal* comoving luminosity densities in summing the LFs over the observed luminosities; in this case there is no assumption made over the bright or faint end of the LF which may be not observable in the lowest or highest redshift bins. Secondly, we derive the *estimated* mean comoving luminosity densities in summing the LFs over all luminosities. As we do not observe the faintest galaxies, the latter estimates are derived by extrapolating the LF obtained using the STY estimator. This approach is the only way to compare data through cosmic epochs since we integrate to the same faintest luminosity, as long as a cut-off at faint luminosities is not observed.

3.3. Uncertainties

The LF parameters are correlated to each other, and the effect of this correlation is that the uncertainty in the LF integral requires the incorporation of the LF parameter error ellipse, in addition to the Poisson uncertainties typically quoted.

Thus for the two correlated parameters, $\alpha - M^*$, the uncertainty of \mathcal{L} is derived from the optimal confidence regions as determined using the STY errors. The error ellipse implies that the uncertainty is not given by the squares of the one-standard-deviation (σ) errors of α and M^* as done in the case of two individual, normally-distributed parameters which give an estimated value within a 68 percent confidence interval. Actually, the correlation increases the errors on the other parameter. Indeed, the probability that α and M^* *simultaneously* take on values with the one- σ likelihood contour is 39 percent only. We use the likelihood contour corresponding to a 68 percent confidence interval, that is at 2.3σ . Using the number counts, we derive ϕ^* for each point of this contour. Our final uncertainties correspond to the

two points of the error contour which give the lowest and highest values of \mathcal{L} .

In this procedure none of the two parameters, α or M^* , has been fixed. If we fix one of the two parameters, then it decreases the errors on the other parameter. In this case, errors are usually not realistic, so we use another method to give uncertainties as follows. We derive $L^* \Gamma(\alpha + 2)$ using the estimated Schechter parameters with the low, high, and mean values chosen for the fixed parameter, and with the 1σ error on the other free parameter. Using the number counts, we derive ϕ^* for each point of the single free parameter axis. In the case of a fixed parameter, we take the extreme uncertainties given by the highest (lowest) \mathcal{L} estimation calculated with the high (low) value of the fixed parameter, and subtracted to the lowest (highest) estimation calculated with the mean value. When we fix either M^* or α , we footnote it in our tables of \mathcal{L} values.

3.3.1. Fixing the Schechter parameter M^*

The brightest galaxies are not sampled in the first redshift bin ($0.05 < z < 0.2$) because of the VVDS bright limit at $I_{AB} = 17.5$. Thus in this redshift range we fix $M^* \pm 0.05$ to its mean local value, as found by the SDSS at $z = 0.1$ in the U , B , V , R , and I bands (Blanton et al. 2003). We gave these values in Sect. 5.1 and Table 1 of Ilbert et al. (2005). In the far-UV band we fix $M^* \pm 0.10$ to the one derived by Wyder et al. (2005) from the GALEX-2dFGRS survey at $\langle z \rangle = 0.055$. The resulting STY parameters are with $M_{\text{fix}}^* = -18.12$ mag, $\alpha = -1.13$, and $\phi^* = 0.00732 \text{ Mpc}^{-3}$.

3.3.2. Fixing the Schechter parameter α

At high redshift ($z > 1.2$), we need to fix α because the VVDS faint limit, $I_{AB} = 24$, prevents us from observing luminosities faint enough to constrain the LF faint-end slope. One of the most important things done to obtain a reliable estimate of \mathcal{L} is to sample the LF around the knee of the luminosity distribution. If we do not observe magnitudes fainter than the LF knee, (i.e. $L < L^*$), then \mathcal{L} is underestimated whatever the value given to α . As long as α is greater than -1 the total luminosity density is little dependent on the slope, as illustrated in Fig. 1, and is dominated by the product of ϕ^* and L^* . For slopes < -1 , and constant $\phi^* \times L^*$, \mathcal{L} increases of 32, 78, and 209 percent from $\alpha = -1$ to -1.3 , -1.5 , and -1.7 , respectively. Thus uncertainties on \mathcal{L} can be quite large when $\alpha < -1.3$. The low, high, and mean values for a fixed slope are described in the appropriate sections.

4. Global luminosity densities at $0 < z < 2$

4.1. The VVDS multi-wavelength data

The Schechter parameters are those derived in Ilbert et al. (2005) in the rest-frame U -3600, B -4400, V -5500, R -6500, and I -7900 passbands from $z = 0.05$ to $z = 1$. In the redshift bins $1.0 < z < 1.3$ and $1.3 < z < 2.0$ we were very cautious in fixing the LF faint-end slope to the value of the slope estimated in the redshift bin $0.8 < z < 1.0$. Now, we estimate the slope in the redshift bin $1.0 < z < 1.2$, and at $z > 1.2$ we use our result from Fig. 9 in Ilbert et al. (2005) illustrating the steepening of the LF faint-end slope with increasing redshift. It corresponds to $\Delta\alpha = 0.3$ between $z \simeq 0.1$ and $z \simeq 0.9$, that is an increase of 0.0375 at each step of 0.1 in redshift. We have fixed α in keeping this increment since there is no reason why it should suddenly stop increasing. In particular, for the bin $1.2 < z < 1.4$ ($\langle z \rangle = 1.3$), we take the

Table 1. Comoving multi-wavelength non dust-corrected luminosity densities at $0 < z < 2$ of the VVDS with the cosmology (Ω_M, Ω_b, h) = (0.3, 0.7, 0.7).

$\langle z \rangle^a$	Redshift range	δt^b	$\log \mathcal{L}_{1500 \text{ \AA}}$	$\log \mathcal{L}_{2800 \text{ \AA}}$	$\log \mathcal{L}_{3600 \text{ \AA}}$	$\log \mathcal{L}_{4400 \text{ \AA}}$	$\log \mathcal{L}_{5500 \text{ \AA}}$	$\log \mathcal{L}_{6500 \text{ \AA}}$	$\log \mathcal{L}_{7900 \text{ \AA}}$
Minimal									
0.14	[0.05–0.20]	2.5	18.65	18.87	19.17	19.62	19.77	19.94	20.05
0.30	[0.20–0.40]	2.0	18.83	19.07	19.31	19.72	19.87	19.99	20.09
0.51	[0.40–0.60]	1.3	18.82	19.11	19.42	19.72	19.91	20.00	20.08
0.69	[0.60–0.80]	1.1	18.99	19.30	19.48	19.84	19.98	20.05	20.13
0.90	[0.80–1.00]	0.9	19.00	19.29	19.47	19.82	19.95	20.02	20.09
1.09	[1.00–1.20]	0.7	18.97	19.33	19.46	19.79	19.92	19.99	20.07
1.29	[1.20–1.40]	0.6	18.91	19.22	19.37	19.68	19.78	19.83	19.92
1.55	[1.40–2.00]	1.3	18.81	19.23	19.36	19.64	19.73	19.78	19.83
Estimated									
0.14	[0.05–0.20] ^c	2.5	18.81 ^{+0.08} _{-0.04}	18.98 ^{+0.07} _{-0.06}	19.23 ^{+0.06} _{-0.06}	19.66 ^{+0.06} _{-0.06}	19.93 ^{+0.04} _{-0.04}	20.07 ^{+0.07} _{-0.07}	20.17 ^{+0.07} _{-0.07}
0.30	[0.20–0.40] ^f	2.0	18.96 ^{+0.14} _{-0.13}	19.10 ^{+0.04} _{-0.03}	19.34 ^{+0.03} _{-0.03}	19.76 ^{+0.06} _{-0.04}	19.96 ^{+0.09} _{-0.06}	20.10 ^{+0.12} _{-0.07}	20.27 ^{+0.26} _{-0.11}
0.51	[0.40–0.60] ^{e,f}	1.3	19.00 ^{+0.35} _{-0.12}	19.17 ^{+0.02} _{-0.06}	19.47 ^{+0.03} _{-0.03}	19.77 ^{+0.04} _{-0.03}	19.97 ^{+0.04} _{-0.04}	20.07 ^{+0.05} _{-0.04}	20.16 ^{+0.07} _{-0.05}
0.69	[0.60–0.80] ^{e,f}	1.1	19.17 ^{+0.10} _{-0.09}	19.33 ^{+0.06} _{-0.03}	19.57 ^{+0.05} _{-0.04}	19.87 ^{+0.02} _{-0.02}	20.03 ^{+0.02} _{-0.02}	20.11 ^{+0.02} _{-0.02}	20.19 ^{+0.03} _{-0.02}
0.90	[0.80–1.00] ^{e,f}	0.9	19.29 ^{+0.12} _{-0.13}	19.48 ^{+0.13} _{-0.11}	19.69 ^{+0.21} _{-0.10}	19.92 ^{+0.03} _{-0.02}	20.07 ^{+0.04} _{-0.03}	20.14 ^{+0.05} _{-0.04}	20.23 ^{+0.06} _{-0.04}
1.09	[1.00–1.20] ^{e,f}	0.7	19.41 ^{+0.16} _{-0.17}	19.47 ^{+0.19} _{-0.11}	19.73 ^{+0.06} _{-0.05}	19.97 ^{+0.03} _{-0.02}	20.13 ^{+0.05} _{-0.04}	20.19 ^{+0.05} _{-0.04}	20.27 ^{+0.07} _{-0.05}
1.29	[1.20–1.40] ^{d,e,f}	0.6	19.35 ^{+0.18} _{-0.22}	19.53 ^{+0.32} _{-0.14}	19.74 ^{+0.09} _{-0.07}	19.87 ^{+0.09} _{-0.04}	20.06 ^{+0.10} _{-0.08}	20.18 ^{+0.09} _{-0.10}	20.26 ^{+0.15} _{-0.12}
1.55	[1.40–2.00] ^{d,e,f}	1.3	19.31 ^{+0.22} _{-0.25}	19.65 ^{+0.46} _{-0.15}	19.74 ^{+0.13} _{-0.10}	19.74 ^{+0.10} _{-0.05}	20.00 ^{+0.15} _{-0.11}	20.14 ^{+0.12} _{-0.18}	20.27 ^{+0.24} _{-0.17}

^a Mean redshift of the galaxy redshifts in the quoted redshift range.^b Elapsed time in Gyr in the redshift bin.^c At $0.05 < z < 0.20$ with $\langle z \rangle = 0.14$ the STY LF estimators are derived using a fixed M^* in the $U, B, V, R,$ and I bands taken from the SDSS ($\langle z \rangle \sim 0.1$, Blanton et al. 2003; see also Sect. 5.1 in Ilbert et al. 2005), in the FUV-1500 band from the GALEX-2dFGRS survey ($\langle z \rangle = 0.055$ Wyder et al. 2005), and in the NUV-2800 from our value estimated at $0.1 < z < 0.3$ (i.e. -18.61 mag) since there is no local value in the literature. Error bars are derived from the STY estimations at $M^* \pm 0.10$ for the FUV and NUV bands, otherwise at $M^* \pm 0.05$.^d At $1.2 < z < 2.0$ the STY LF estimators are constrained using a fixed α and error bars are derived from the STY estimations at $\alpha \pm 0.0375$ as detailed in Sect. 4 except for the FUV and NUV bands (see below).^e In the NUV the slope is fixed to the value estimated at $0.2 < z < 0.4$, i.e. $\alpha = -1.32$. Error bars are derived from the STY high estimations assuming an increase of α , of $+0.0375$ each 0.1 redshift bin, as observed in the visible (see Sect. 4), and from the STY low estimations assuming $\alpha = -1$ at $0.8 < z < 2$, and from the minimal value at $0.4 < z < 0.8$ since in this redshift range the latter is higher than the STY estimate assuming $\alpha = -1$.^f In the FUV the slope is fixed to $\alpha = -1.60$ at $0.2 < z < 2$ corresponding to the slope found with the GALEX-VVDS sample (Arnouts et al. 2005). Error bars are derived from the STY estimations assuming $\alpha = -1.20$ and $\alpha = -1.75$, which corresponds to the large range of values found in the literature due to the lack of constraint on the faint end slope of the LF.

value of α measured in the bin $1.0 < z < 1.2$ ($\langle z \rangle = 1.1$) and we increase it by $2 \times 0.0375 = 0.075$. For the bin $1.4 < z < 2.0$ ($\langle z \rangle = 1.5$), we take the value of α in the bin $1.2 < z < 1.4$ ($\langle z \rangle = 1.3$) and we increase it by 0.075 also. In these two redshift bins, we assume ± 0.075 for the error bars of the fixed α values.

We have derived the rest-frame FUV-1500 and NUV-2800 luminosity densities. While the rest-frame 2800 Å luminosities are sampled by the observed reference bands from U -band to I -band from $z = 0.3$ to $z = 2.0$, the rest-frame 1500 Å luminosities are sampled only at $z > 1.4$. Our LFs computed at 1500 Å therefore strongly rely on the spectral energy distribution (SED) fit at longer wavelengths. However, in Arnouts et al. (2005) we have already derived the 1500 Å LFs using data from GALEX (Martin et al. 2005). These data were a ($NUV-2300+I$)-selected GALEX-VVDS sample from $z = 0.2$ to $z = 1.2$ and they were mainly based on a one-to-one identification between optical images and NUV images. Our present FUV results are SED-dependent but derived from a pure I -selected sample similar to what was done in the other bands. At $0.2 < z < 0.8$ the I -selected VVDS and the ($NUV + I$)-selected GALEX-VVDS LFs are in agreement within the error bars. This implies that even though our FUV result is SED dependent, our SED fitting is globally correct using a fixed -1.6 slope at $0 < z < 2$. At $0.8 < z < 1.2$,

the two FUV luminosity densities differ significantly of ~ 0.2 dex because of a lower ϕ^* for the ($NUV + I$)-selected sample. The weights we adopted in Arnouts et al. (2005) were preliminary and slightly underestimated at $0.8 < z < 1.2$.

Values of \mathcal{L} for each passband in various redshift bins are given in Table 1, and they are displayed in Figs. 2–4 for the B, V, R and $I,$ and U and NUV and FUV bands, respectively.

4.2. Evolution according the rest-frame passband

The dependence of the emissivity of the global population on the rest-frame band is noticeable. The non dust-corrected luminosity densities evolve with redshift over $0.05 \leq z \leq 1.2$, as $\mathcal{L} \propto (1+z)^x$ with $x = 2.05, 1.94, 1.92, 1.14, 0.73, 0.42,$ and 0.30 in FUV-1500, NUV-2800, $U-3600, B-4400, V-5500, R-6500,$ and $I-7900$ passbands, respectively (see Figs. 2–5). There is a clear differential, wavelength-dependent evolution of the whole population. Indeed, the average (FUV–I) rest-frame color emissivity of the whole galaxy population becomes four times redder from $z = 1.2$ to nowadays. Furthermore, the data suggest an up-turn in the emissivity evolution at redder wavelengths than the I -band. Nevertheless a possible up-turn is likely a selection effect due to the fact that the rest-frame I -band emissivities from an

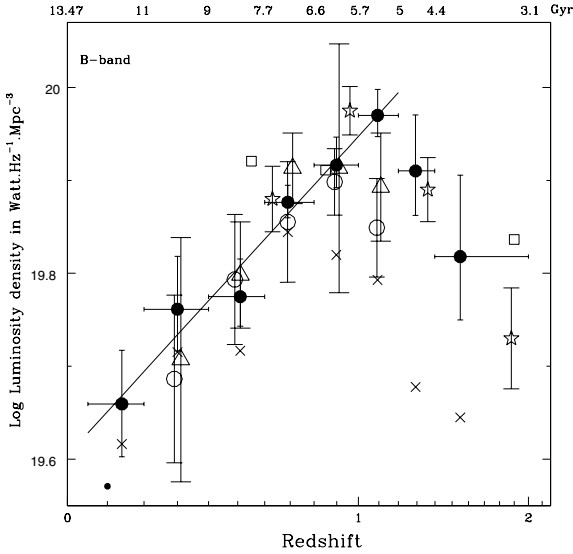


Fig. 2. The *estimated* non dust-corrected comoving luminosity densities in the rest-frame B -4400 passband as a function of $\log(1+z)$ and represented with *filled circles*. The *crosses* are the *minimal* comoving densities, derived from the observed luminosities without extrapolation neither at the bright nor at the faint part of the LF. Data are displayed at the mean redshift of the galaxies within each redshift bin. Error bars are derived from the 2.3σ error contours of the Schechter parameters, except at $z < 0.2$ where M^* is fixed and at $z > 1.2$ where α is fixed. The *dot* at $z = 0.1$ is the SDSS local point. The VVDS B -band luminosity densities increase as $(1+z)^{1.14}$ up to $z = 1.1$. Data are listed in Table 1. The *open triangles* and *open circles* are the DEEP2 and COMBO-17 data displayed for clarity at -0.05 and $+0.05$ in redshift respectively and taken from Table 2 in Faber et al. (2005), the *open squares* are the HDF data from Poli et al. (2003), and the *open stars* are the FDF data from Gabasch et al. (2004).

I -selected sample could be underestimated in missing the very red galaxies at $z > 1$.

The FUV is related to the formation of young, massive, short-lived, hot stars, while the NIR is related to long-lived, old stars which relate closely to the stellar mass of a galaxy. And thus, over the last 8.5 Gyrs ($z < 1.2$) there has been a substantial decline of the star formation rate, while the old stellar content shows a smoother change in terms of emissivity. In Pozzetti et al. (2007), we derive the stellar masses using a rest-frame K -band sample, and we conclude that at $z < 1$ the stellar mass density increases by a factor of ~ 2.3 . Since the global rest-frame ultraviolet emissivity continues to decline, merger events should produce little star formation, either via minor mergers with e.g. satellite galaxy accretion, or via majors mergers between cold gas-depleted galaxies so there is not enough gas to efficiently produce new stars.

At $z \sim 1.1$ our luminosity densities exhibit a transition in the evolutionary trend. In particular, from $z = 2$ to $z = 1.2$, the FUV -, B -, V - and R -band \mathcal{L} increase, the U - and I -band \mathcal{L} flatten; and then below $z = 1.2$, they all decrease. Only the NUV \mathcal{L} follows a continuous evolution since $z = 2$. Nevertheless, error bars at $z > 1.2$ are large, and thus the observed transition is still uncertain.

5. Comparison with other surveys

5.1. Comparison with the CFRS at $I_{AB} = 22.5$

The CFRS is an I -selected survey like the VVDS. The CFRS galaxy sample consists of 730 I -band selected galaxies at $17.5 \leq I_{AB} \leq 22.5$, of which 591 (i.e., more than 80 percent) have

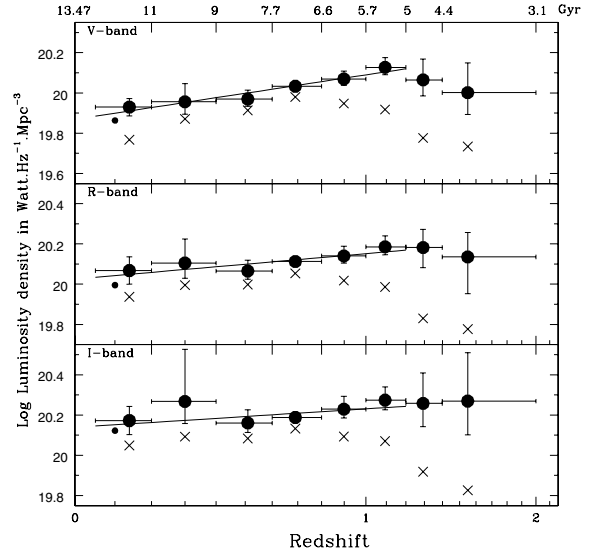


Fig. 3. Comoving non dust-corrected luminosity densities in the rest-frame V -5500, R -6500, and I -7900 passbands. The *filled circles*, *crosses*, and the *dot* are the same as in Fig. 2. The VVDS V -, R -, and I -band densities increase as $(1+z)^{0.73}$, $(1+z)^{0.42}$, and $(1+z)^{0.30}$ up to $z = 1.1$ respectively.

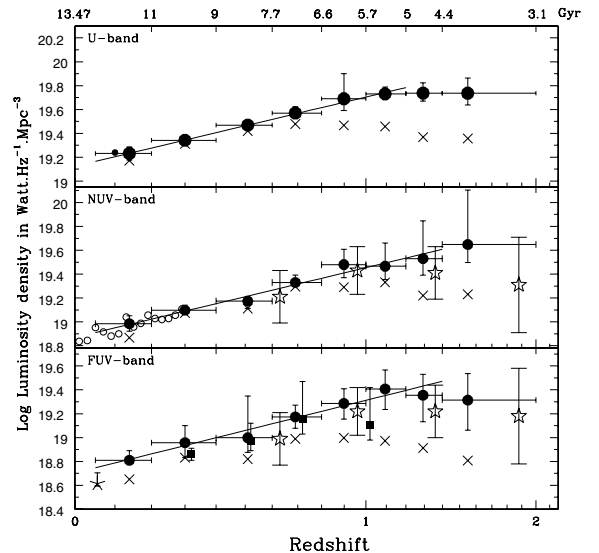


Fig. 4. Comoving non dust-corrected luminosity densities in the rest-frame U -3600, NUV-2800, and FUV-1500 passbands. The *filled circles*, *crosses*, *open stars*, and the *dot* come from the same data as in Fig. 2. The VVDS U -, NUV-, and FUV-band densities increase as $(1+z)^{1.92}$, $(1+z)^{1.94}$, and $(1+z)^{2.05}$ up to $z = 1.1$ respectively. The *asterisk* is the FUV-band local point from the GALEX-2dFGRS survey ($\langle z \rangle = 0.055$ Wyder et al. 2005). The *plain squares* are the FUV-band data, displayed for clarity at $+0.02$ in redshift, and taken from the GALEX-VVDS survey (Schiminovich et al. 2005). The *small open circles* are the NUV-band points from the SDSS (Baldry et al. 2005).

reliable redshifts in the range $0 < z < 1.3$ (Le Fèvre et al. 1995). Lilly et al. (1996) estimated the comoving luminosity densities of the Universe from the CFRS sample in the rest-frame NUV-2800, B -4400, and NIR-10 000 passbands over the redshift range $0 < z < 1$ with the cosmology $(\Omega_M, \Omega_\Lambda, h) = (1, 0, 0.5)$. Here, we compare with the B -band results which require very little extrapolation from models, contrary to the NUV or NIR data. From the best estimate of the B -4400 band LF (see Lilly et al. 1995), the rest-frame B -band emissivities directly-observed

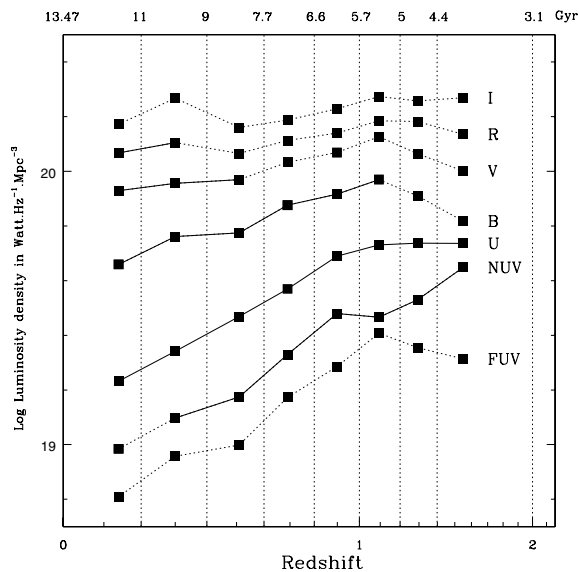


Fig. 5. Comoving non dust-corrected VVDS luminosity densities in the rest-frame FUV-1500, NUV-2800, U -3600, B -4400, V -5500, R -6500, and I -7900 passbands from bottom to top respectively, as displayed in Figs. 2–4. The solid line connects points where the rest-frame band is observed in the optical.

(correspond to our minimal estimates) and estimated were derived. The CFRS estimated $\mathcal{L}_{4400 \text{ \AA}}$ was derived fitting with a Schechter function the data given by the V_{max} LF estimator. The VVDS estimated $\mathcal{L}_{4400 \text{ \AA}}$ is derived from the integration of the LF estimate with α , M^* , and ϕ^* as determined with the STY method. The two fits give similar results as long as each type of galaxies is visible within the redshift range studied (see Ilbert et al. 2004).

The upper panel of Fig. 6 compares the CFRS $\mathcal{L}_{4400 \text{ \AA}}$ to the VVDS $\mathcal{L}_{4400 \text{ \AA}}$ with a magnitude cut at $I_{AB} = 22.5$ over the same redshift range, $0.2 \leq z \leq 1.0$, and with the same cosmology adopted in the CFRS analysis. The CFRS and the VVDS-[17.5–22.5] $\mathcal{L}_{4400 \text{ \AA}}$ are very well consistent with each other (see Table 2). Even though the CFRS contains ~ 4.5 times fewer galaxies than the VVDS at the same depth, the CFRS error bars are smaller than the VVDS error bars. This is due to different procedures used to estimate the uncertainties in the two surveys. The CFRS “ad-hoc” uncertainty procedure is described in Lilly et al. (1996), and ours are derived from the $\alpha - M^*$ error contour of 68 percent confidence level of our STY estimate. In both surveys, the minimal and the estimated B -band emissivities become more discrepant as the redshift increases. This is due to the combination of brighter limiting luminosities sampled at higher redshifts, and to a lesser extent, a steeper faint-end slope of the rest-frame B -band LF. The CFRS $0.2 < z < 1.0$ values are thus found to be very reliable up to $I_{AB} = 22.5$.

5.2. From the CFRS to the 1.5 mag deeper VVDS

The lower panel of Fig. 6 compares the VVDS $\mathcal{L}_{4400 \text{ \AA}}$ cut at $I_{AB} = 22.5$ with the global VVDS at $I_{AB} = 24.0$ over the same redshift range, $0.2 \leq z \leq 1.0$, and with the same cosmology as the CFRS. In the redshift range, $0.2 < z < 1.0$, $\mathcal{L}_{4400 \text{ \AA}}$ from the global VVDS is consistent within the error bars with the one from the VVDS-[17.5–22.5] (see Table 2). Our VVDS local value at $z = 0.138$ is derived by fixing M^* to the SDSS value, $(-19.30 - 5 \log h)$ mag at $z = 0.1$ (see Table 2 in Blanton et al. 2003, with $^{0.1}g$ -band $\approx B$ -band at less than a 0.05 mag difference level), since we do not span the brightest luminosities at $z < 0.2$.

In this redshift range, we observe fainter luminosities than the SDSS, and we find a steeper faint-end slope than the SDSS (see discussion in Sect. 5.1 in Ilbert et al. 2005).

The best fit power law for the estimated $\mathcal{L}_{4400 \text{ \AA}}$ of the VVDS data gives $(1+z)^{2.05 \pm 0.06}$ to be compared with the one of the CFRS, $(1+z)^{2.72 \pm 0.5}$ (see Lilly et al. 1996) in cosmology $(\Omega_M, \Omega_\Lambda, h) = (1, 0, 0.5)$. The steeper slope of the CFRS data is due to the combination of the adopted low local reference at $z = 0$ and the high normalization of the CFRS LF at $z = 0.85$ due to a poor constraint of α and M^* with a sample limited at $I_{AB} = 22.5$.

The CFRS $\mathcal{L}_{2800 \text{ \AA}}$ evolution was found as $(1+z)^{3.9 \pm 0.75}$ (see Lilly et al. 1996). With the same cosmology $(\Omega_M, \Omega_\Lambda, h) = (1, 0, 0.5)$ and $I_{AB} < 24$ the VVDS $\mathcal{L}_{2800 \text{ \AA}}$ evolves as $(1+z)^{2.4 \pm 0.1}$. The rest-frame NUV -2800 is observed in the optical in the VVDS at $z > 0.2$, while in the CFRS it is observed at $z > 0.5$. It adds uncertainties due to the extrapolation of templates. Thus the NUV CFRS evolution was found too steep as it was already seen by Wilson et al. (2002).

In conclusion we find that the B -band luminosity density estimated from the VVDS is in excellent agreement with that estimated from the CFRS at $0.2 < z < 0.75$ (see Table 2). We demonstrate that going deeper in magnitude is superior to assembling larger samples as far as the galaxy sample is not dependent on cosmic variance and has a well-defined selection function. Furthermore, comparing the estimates of the VVDS at 22.5 mag to the ones of the VVDS at 24 mag shows that the error bars determined in the VVDS are well-defined. Indeed the estimate at 24 mag is within the error bars of the one at 22.5 mag since we account for the uncertainty on the LF slope. Finally, we confirm that the uncertainties due to template extrapolation led to the very steep slope of the NUV CFRS luminosity density evolution.

5.3. Comparison with other deep surveys

In Fig. 2 we added the B -band luminosity densities from DEEP2 and COMBO-17 surveys (values taken in Table 2 in Faber et al. 2005), from the FORS Deep Fields (FDF) survey where Schechter parameters are taken from Table A.5 in Gabasch et al. (2004), and from the HDF survey where Schechter parameters are taken from Table 2 in Poli et al. (2003). These surveys at $0.2 < z < 1$ are in excellent agreement with the VVDS, except for the Poli et al. (2003) at $0.4 < z < 0.7$ which has a steeper faint-end slope ($\Delta\alpha \sim 0.15$) than the VVDS, and thus presents a B -band \mathcal{L} higher by 0.1 dex than the other surveys in this redshift range. At $1 < z < 1.2$ the VVDS is higher by 0.1 dex than DEEP2 because the faint-end slope of the B -band LF is better constrained in the VVDS, a deeper sample by ~ 1 mag than DEEP2. We note that both the I -selected VVDS and the deeper by 2.8 mag I -selected FDF exhibit a drop of the B -band luminosity density at $z \gtrsim 1.1$.

Our 1500 \AA \mathcal{L} results are slightly higher than the ones from the FDF by 0.1 dex at $0.6 < z < 2$. It is likely due to their lower fixed ($\alpha = -1.07$) value than our fixed ($\alpha = -1.6$) value. However, the difference is usually within the error bars. Our 2800 \AA \mathcal{L} results are in good agreement with the ones from the FDF at $0.4 < z < 1.2$, and in excellent agreement with the ones from the SDSS (Baldry et al. 2005) at $z < 0.3$.

6. Luminosity densities per galaxy type at $z < 2$

6.1. The VVDS galaxy types

The large VVDS sample enables us to study the luminosity density evolution for different galaxy types. To associate a spectral

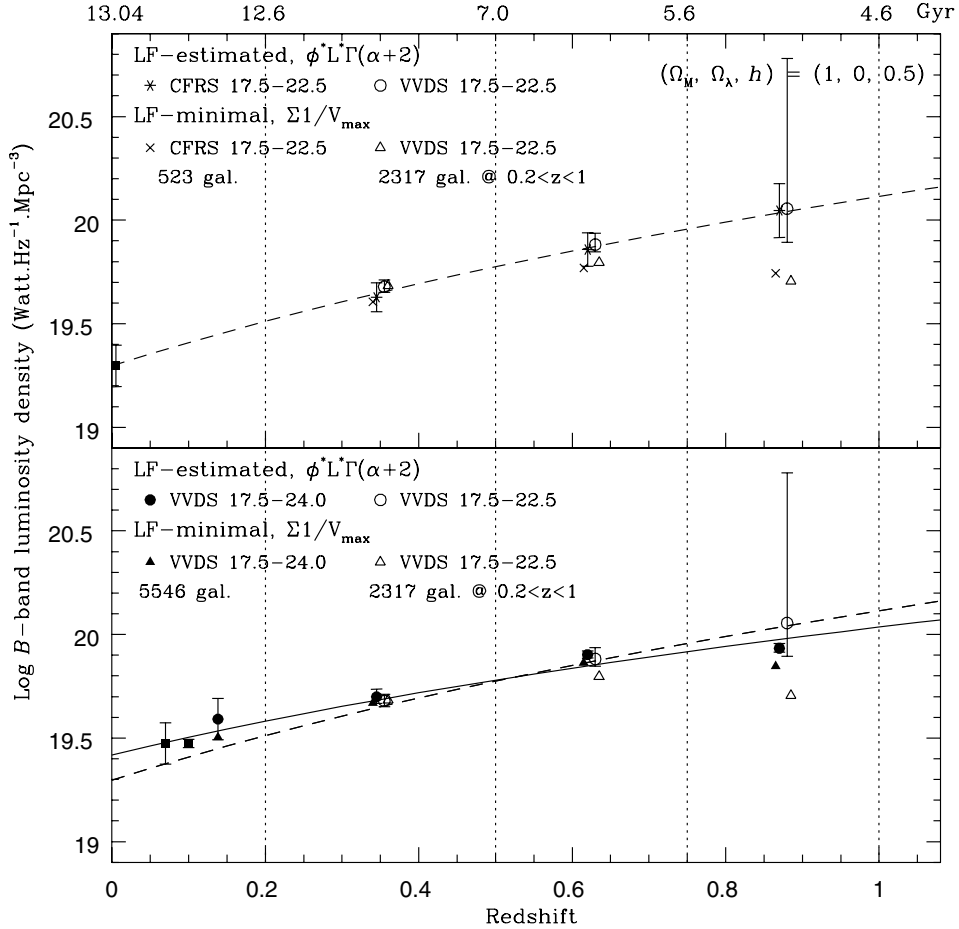


Fig. 6. Rest-frame B -band comoving non dust-corrected luminosity densities with the $(\Omega_M, \Omega_\Lambda, h) = (1, 0, 0.5)$ cosmology at $0 < z < 1$ of the I -selected CFRS and VVDS surveys. Values are listed in Table 2. For clarity the $z > 0.2$ data are represented by symbols slightly displaced horizontally from the center of the redshift bins delimited with the vertical dotted lines. The plain square points at $z = 0.05, 0.07$, and 0.1 are local points from the SAPM (Loveday et al. 1992), the 2dFGRS (Norberg et al. 2002), and SDSS (Blanton et al. 2003) respectively. The dashed line shows the best-fit power law and its associated uncertainties for the “LF-estimated” $\mathcal{L}_{4400, \text{\AA}}$ of the CFRS 17.5–22.5 data derived in Lilly et al. (1996), $(1+z)^{2.72 \pm 0.5}$, and the solid line is the one for the VVDS 17.5–24.0 data, $(1+z)^{2.05 \pm 0.06}$.

Table 2. Comparison of comoving luminosity densities between I -selected surveys, the CFRS and VVDS, with the cosmology $(\Omega_M, \Omega_\Lambda, h) = (1, 0, 0.5)$.

Redshift range	$\log \mathcal{L}_{4400, \text{\AA}}$ in $\text{W Hz}^{-1} \text{Mpc}^{-3}$		
	CFRS [17.5–22.5]	VVDS [17.5–22.5]	VVDS [17.5–24.0]
	Minimal		
$z < 0.2$	–	–	19.50 ± 0.03^a
0.20–0.50	19.61 ± 0.07	19.68 ± 0.01	19.67 ± 0.01
0.50–0.75	19.77 ± 0.07	19.80 ± 0.02	19.86 ± 0.01
0.75–1.00	19.74 ± 0.07	19.71 ± 0.01	19.85 ± 0.01
	Estimated		
$z < 0.2$	19.30 ± 0.10^b	–	$19.59^{+0.10}_-0.10^a$
0.20–0.50	19.63 ± 0.07	$19.68^{+0.03}_-0.03$	$19.70^{+0.04}_-0.03$
0.50–0.75	19.86 ± 0.08	$19.88^{+0.05}_-0.05$	$19.90^{+0.02}_-0.02$
0.75–1.00	20.05 ± 0.13	$20.06^{+0.02}_-0.16$	$19.93^{+0.02}_-0.02$

^a With M^* fixed to the SDSS $^{0.1}g$ -LF estimate from Blanton et al. (2003) (B -band \sim $^{0.1}g$ -band with less than 0.05 mag difference).

^b Based on SAPM b_j -LF estimate from Loveday et al. (1992).

type to our galaxies with a known spectroscopic redshift, we used the best fitting type between $UBVRI$ photometric data and a

set of SEDs that were lineary interpolated between the four observed spectra of Coleman et al. (1980), i.e. E/S0, Sbc, Scd, and Irr, and two starburst models from the GISSEL library (Bruzual & Charlot 1993). Then we divided the galaxy population into four rest-frame color classes, the elliptical-like (*type-1*), the early spiral-like (*type-2*), the late spiral-like (*type-3*), and the irregular-like (*type-4*) types. We describe in detail in Zucca et al. (2006) the fitting process and the robustness of the classification.

We note that several previous deep surveys were limited to the study of two population sub-samples. For instance in the CFRS, Lilly et al. (1995) studied blue and red populations, simply dividing the galaxy population into two equal number sub-samples and corresponding to a Sbc color separation. This allowed us to identify little evolution of the red population while the blue population evolves strongly. In more recent deep surveys, the bimodal rest-frame color distribution observed at least up to $z = 1.5$ is being used to define an empirical separation between red and blue galaxies (K20; Fontana et al. 2004, DEEP2 and COMBO-17; Faber et al. 2005, VVDS; Franzetti et al. 2007). While the bimodality is clearly observed for the bright galaxies, the faint population does not exhibit two contrasting modes (see Franzetti et al. 2007). Also, the bimodality hides a strong differential, color evolution of the bright population (i.e. $L > L^*$) as shown in Fig. 2 of Zucca et al. (2006). Or, the

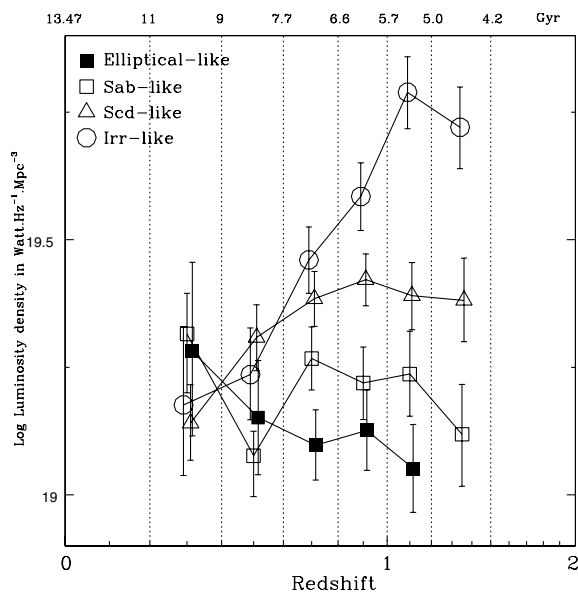


Fig. 7. Comoving non dust-corrected luminosity densities in the rest-frame B -passband from early to late galaxy types (see details in Sect. 6.1). For clarity, data are represented by symbols slightly displaced horizontally from the center of the redshift bins. Error bars are at 1σ . The irregular-like type emissivity decreases markedly by a factor 4, while the elliptical-like type increases by a factor 1.7 from $z = 1.1$ to $z = 0.2$. We note that at $z < 0.4$ the total emissivity is dominated by the early-type population.

extensive analysis of De Lapparent (2003) shows that estimations of LFs based on two color sub-samples lacks the necessary discriminatory power for detecting the variations in luminosity as a function of type which are traced by the intrinsic LFs. From a theoretical study using semi-analytical models, Kaviraj et al. (2006) show that the red-sequence traces the progenitor set of early-type galaxies in terms of numbers and masses for the bright galaxies, but breaks down severely at faint ($L < L^*$) luminosities. And thus, using the bimodality does not seem to be robust in classifying galaxies in types unambiguously related to passively evolving galaxies on one side and star-forming galaxies on the other. Whereas, in fact, our selection relies on the complete SED available from the multi-band imaging. We note that Seyfert 2 galaxies are included in our sample. We analyse these galaxies with the true starburst population in another paper. Nevertheless we do not expect a large contribution of the Seyfert 2 population at $z < 1$.

We emphasize that our four types are nicely correlated with colors and asymmetry-concentration parameters from HST images (see Fig. 2 in Ilbert et al. 2006a) and with spectroscopic features (e.g. emission line strength, 4000 Å break, see Fig. 1 in Zucca et al. 2006). The four individual LFs were derived between $0.2 < z < 1.5$ where our sample is essentially complete for every type, and Fig. 7 displays the four luminosity densities in the rest-frame B -band where there is very little extrapolation.

6.2. Evolution of \mathcal{L} per type

The evolution of the B -band LF per type and the evolution of the fraction of bright ($M_{B_{AB}} - 5 \log(h) < -20$) galaxies has been described in detail in Zucca et al. (2006), and consequently, the B -band luminosity densities evolve as follows.

Type-4: irregular, starburst, very blue galaxies. The fraction of bright galaxies decreases from ~ 35 to ~ 5 percent from

$z = 1.5$ to $z = 0.2$. The LF undergoes a strong evolution in density (negative) and luminosity (negative). There is a strong decrease in volume density by a factor ~ 2 coming from both the bright and faint parts of the LF. And thus \mathcal{L} decreases markedly from $z = 1.5$ to $z = 0.2$, by a factor ~ 3.5 .

The three other types have an LF which corresponds to a mild evolution in density (positive) and luminosity (negative).

Type-3: late-spirals, star forming, blue galaxies. The fraction of bright galaxies decreases from ~ 40 to ~ 10 percent from $z = 1.5$ to $z = 0.2$, and meanwhile the \mathcal{L} decreases by a factor ~ 1.7 . To keep decreasing $\phi^* \times L^*$ this population is strongly faintening by ~ 1.5 mag. \mathcal{L} decreases markedly at $z < 0.4$ by a factor ~ 1.5 due to the faintening by ~ 1 mag of the LF.

The last two types present an increasing fraction of bright galaxies.

Type-2: early-spirals, post-starburst, red galaxies. The fraction of bright galaxies increases from ~ 20 to ~ 35 percent from $z = 1.5$ to $z = 0.2$, and globally \mathcal{L} increases by a factor ~ 1.6 . To keep increasing $\phi^* \times L^*$ luminous red galaxies must appear at low redshifts since this population is modestly faintening by ~ 0.6 mag. Nevertheless there is a significant variation at low z . Indeed, \mathcal{L} increases from $z = 1.5$ to $z = 0.6$, by a factor ~ 1.4 , then decreases from $z = 0.6$ to $z = 0.4$, by a factor ~ 1.3 , and finally increases from $z = 0.4$ to $z = 0.2$, by a factor ~ 1.7 . This transition implies that a small fraction of luminous type-2 galaxies disappears (~ 13 percent) while the luminosity decreases by a small factor of ~ 0.15 mag.

Type-1: elliptical, red galaxies. The fraction of bright galaxies increases from ~ 0.05 to ~ 55 percent from $z = 1.5$ to $z = 0.2$, and meanwhile \mathcal{L} increases continuously, by a factor ~ 1.7 . That is luminous red galaxies must appear at low redshifts to keep increasing $\phi^* \times L^*$ since this population is faintening by ~ 0.3 mag only.

In addition, Fig. 7 shows that the *type-1* and *type-2* red populations dominate the total light at $z < 0.4$, while at $0.4 < z < 1.2$ the late-type does. Since we know that red spheroids are the majority of our *type-1* population from our work in Ilbert et al. (2006a), we conclude that a dust deficient population is dominant at $z < 0.4$. The luminosity density increasing of the *type-1* and *type-2* red populations suggests a contribution from merging phenomena. Indeed in a downsizing scenario where luminous red galaxies are already in place at high redshifts ($z \gg 1$), and low luminosity red galaxies appear at low redshifts, a flat luminosity density would be expected as a function of redshift, whilst adding merging would increase the luminosity density of the luminous red population as redshift decreases.

We note also that from $z = 0.7$ to $z = 0.5$, \mathcal{L} for *type-2* decreases by a factor ~ 1.3 , while \mathcal{L} for *type-1* increases by a factor ~ 1.15 ; this might suggest that < 15 percent of ellipticals are formed from early-spiral major mergers within this 1.3 Gyr period. It might be evidence for mergers between gas-deficient bright galaxies. Furthermore, the fact that the *type-2* population luminosity density increases again from $z = 0.5$ to $z = 0.3$ by a factor ~ 1.7 might suggest a density growth due of an evolution of *type-4* galaxies towards *type-2* galaxies.

The \mathcal{L} decreasing of the *type-4* population is markedly different from that of the remaining population. This population is dominated by dwarf galaxies (see Zucca et al. 2006). The evolution of this population supports a downsizing scenario where most star formation is shifting to low-mass galaxies at $z < 1.2$, while the global luminosity density is dominated by other galaxy types.

Table 3. STY parameters for the rest-frame FUV-1500 LFs of the *extended* $2.7 < z < 5$ data set.

$\langle z \rangle^a$	Redshift range	α^b fixed	M_{AB}^* (1500) mag Unweighted	ϕ^* (10^{-4} Mpc $^{-3}$)
3.04	[2.70–3.40]	-1.6; -1.2; -1.75	-21.68; -21.46; -21.76	6.27; 8.02; 5.66
3.60	[3.40–3.90]	-1.6; -1.2; -1.75	-22.52; -22.38; -22.84	2.64; 3.45; 1.56
4.26	[3.90–5.00]	-1.6; -1.2; -1.75	-22.72; -22.44; -22.86	0.63; 0.92; 0.50
Incompleteness-corrected ^c				
3.46	[3.00–4.00]	-1.4; -1.2; -1.75	-21.38; -21.29; -21.57	1.23; 1.32; 1.00

^a Mean redshift of the galaxy redshifts in the quoted redshift range.

^b We fixed α to -1.6, -1.2, and -1.75 and the corresponding STY values for M^* and ϕ^* are given, respectively.

^c See Paltani et al. (2007). With $\alpha = -1.6$, we have $M^* = -21.49$ and $\phi^* = 1.11$.

Table 4. Comoving FUV-1500 luminosity densities at $2.7 < z < 5$ of the VVDS for the *extended* high- z dataset.

$\langle z \rangle^a$	Redshift range	δt^b	$\log \mathcal{L}_{1500 \text{ \AA}}$ W Hz $^{-1}$ Mpc $^{-3}$
Unweighted minimal			
3.04	[2.70–3.40]	0.6	18.82
3.60	[3.40–3.90]	0.3	18.95
4.26	[3.90–5.00]	0.3	18.89
Unweighted estimated			
3.04	[2.70–3.40] ^c	0.6	19.47 $^{+0.30}_{-0.33}$
3.60	[3.40–3.90] ^c	0.3	19.43 $^{+0.21}_{-0.29}$
4.26	[3.90–5.00] ^c	0.3	18.89 $^{+0.29}_{-0.29}$
Incompleteness-corrected estimated			
3.46	[3.00–4.00] ^d	0.5	19.47 $^{+0.37}_{-0.11}$

^a Mean redshift of the galaxy redshifts in the quoted redshift range.

^b Elapsed time in Gyr in the redshift bin.

^c The STY LF estimators are derived using a fixed $\alpha = -1.6$ and error bars are derived from the STY estimations assuming $\alpha = -1.20$ and $\alpha = -1.75$ as done at $z < 2$ (see Table 1).

^d In Paltani et al. (2007), we use $\alpha = -1.4$. Here, we use the same minimal and maximum values as at $z < 2$ for α , i.e. -1.2 and -1.75. With $\alpha = -1.60^{+0.15}_{-0.20}$, we find $\log \mathcal{L} = 19.64^{+0.20}_{-0.28}$.

7. Global FUV luminosity densities at $2.7 < z < 5$

7.1. The VVDS high- z population

In the high-redshift range, $2.7 < z < 5.0$, the rest-frame 1500 Å corresponds to the observed frames R and I passbands. Thus uncertainties on absolute magnitudes related to k -corrections and galaxy types are small. Our data set consists of 161 redshifts with VVDS quality flags 2, 3, and 4, and 237 redshifts with VVDS quality flags 1 in the VVDS-0226-04 field (~ 0.5 deg 2). The latter fraction is not negligible since the difficulty in determining a redshift is increased at the faintest apparent magnitudes. The confidence levels for the single high- z population are >50 percent for the flags 2, 3, and 4 dataset, and ~ 45 percent for the flags 1, 2, 3, and 4 dataset (Le Fèvre et al. 2005b).

Here, we correct our sample for the target sampling rate only (see Sect. 2). That is, there is no assumption for the redshift distribution of the sources that were not spectroscopically observed or for which no redshift could be reliably identified from the spectrum obtained. This is a more restricted approach than what was adopted in Ilbert et al. (2005), where the photometric redshifts were used to obtain a spectroscopic success rate as a function of redshift, and thus to correct further for incompleteness. We could not use the same approach here because our photometric redshifts have been thoroughly tested only up to $z \sim 2$

(Ilbert et al. 2006c). The correction for incompleteness has for effect to steepen the slope of the unweighted LF, and since α is correlated with M^* , it produces a brightening (see Fig. 4 in Ilbert et al. 2005).

We consider the two following high- z datasets. The *standard* dataset is composed of quality flags 2, 3, and 4 redshifts and the *extended* dataset is composed of quality flags 1, 2, 3, and 4 redshifts. It is likely that the true luminosity function/density lies between these two cases, assuming that the 7 percent of flags 0 over the whole $0 < z < 5$ sample makes little difference. Using one field of view is likely to induce uncertainty due to cosmic variance. Nevertheless Sawicki & Thompson (2006a) observed an effective area of 169 arcmin 2 , i.e. one third of ours, 410 arcmin 2 , split into five fields (the Keck Deep Fields; KDF) and found a quite moderate cosmic-variance effect.

In Paltani et al. (2007) we do a comprehensive study about the impact of the large uncertain redshift population at $3 < z < 4$, in using a somewhat different analysis. Here we choose to use the same analysis as at $z < 2$. We note that results are qualitatively similar.

7.2. Estimation of the high- z FUV VVDS luminosity functions and densities

For the rest-frame FUV analysis, we fixed α to -1.6. As shown in Fig. 1 the uncertainty in a slope $\alpha < -1.3$ may lead to large discrepancies in the estimation of \mathcal{L} . For consistency, we have derived error bars of the rest-frame FUV \mathcal{L} from the STY estimations assuming $\alpha = -1.20$ and $\alpha = -1.75$ for the *extended* high- z data set as we did at $z < 2$. The LF parameters are given in Table 3. Figure 8 displays the LF estimations of the *standard* and *extended* high- z datasets, and the incompleteness-corrected LF estimated at $3 < z < 4$ in Paltani et al. (2007). We do a detailed comparison for different fixed α values found in the literature in Paltani et al. (2007). The rest-frame FUV \mathcal{L} at $2.7 < z < 5$ are displayed in Fig. 9 together with those at $z < 2$, and they are listed in Table 4.

7.3. Comparison with other high- z surveys

Figure 9 displays other rest-frame FUV luminosity densities from the literature. At $2 < z < 5$, our I -selected rest-frame FUV \mathcal{L} are broadly in agreement with the other estimations. At $z \sim 3$, rest-frame FUV \mathcal{L} estimations are found within 0.1 dex (19.47 for the VVDS; 19.58 for Steidel et al. 1999; 19.43 for Gabasch et al. 2004; 19.52 Arnouts et al. 2005, and 19.51 for Sawicki & Thompson 2006b). We note that the luminosity functions exhibit noticeable discrepancies, in particular at the bright end, and furthermore that the faint end slope is not constrained (see

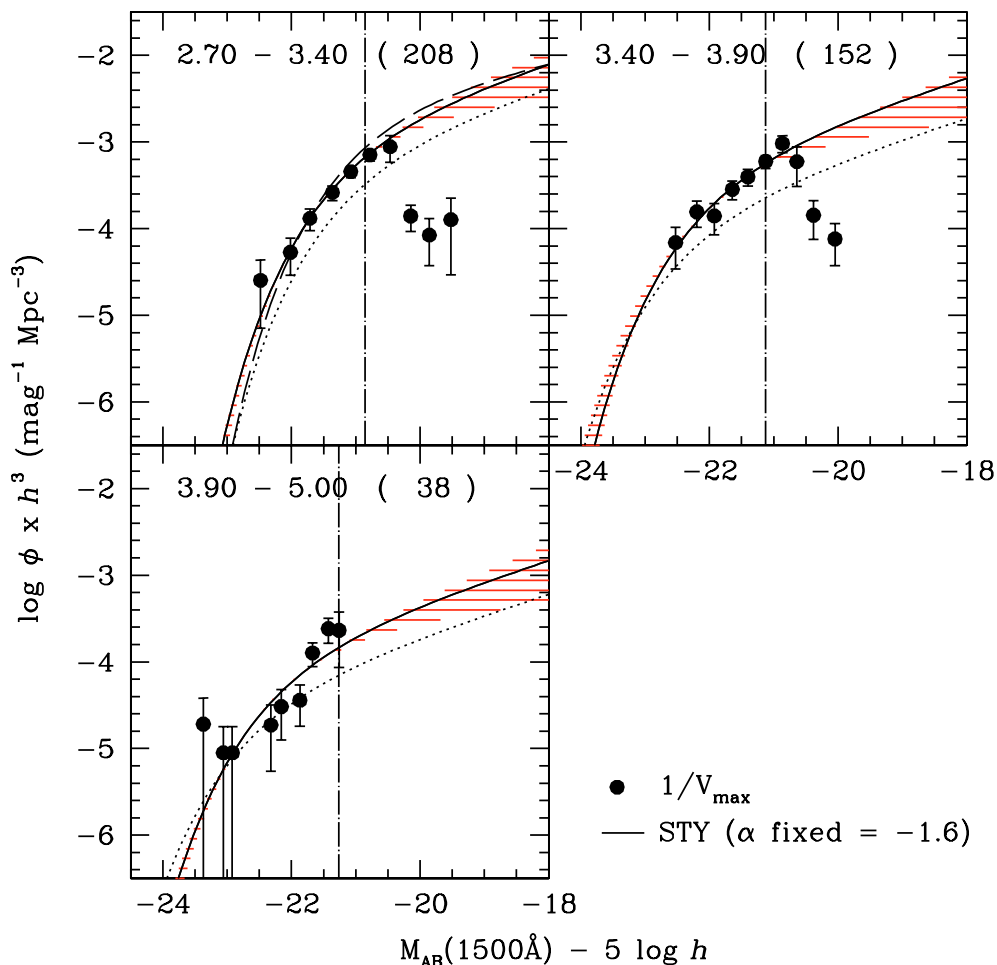


Fig. 8. Unweighted non dust-corrected luminosity functions in the rest-frame FUV-1500 passband estimated with α fixed to -1.60 . The circles and the solid line represent the V_{\max} and the STY estimates for the *extended* dataset where the number of galaxies is given within parenthesis next to the redshift range. The vertical dot-dashed line corresponds to the faint absolute magnitude limits considered in the STY estimate (see Sect. 3.2). The hashed area is limited by the LFs derived with α fixed to -1.20 and -1.75 . The dotted lines represent the STY estimates with α fixed to -1.60 for the *standard* dataset. The *standard* dataset LF is below the *extended* dataset LF since it does not include quality flags 1 (see Sect. 7.1). In the top-left panel, the long-dashed line is the incompleteness-corrected dataset FUV-1500 LF at $3 < z < 4$ derived as in Paltani et al. (2007), with fixed $\alpha = -1.4$.

detailed comparisons in Paltani et al. 2007). As at $z < 2$, our high- z luminosity densities are slightly higher than those estimated from the FDF (due to their lower adopted slope of $\alpha = -1.07$) except at $3.9 < z < 5$. The decrease from $z = 3.4$ to $z = 5$ is smaller in the FDF (0.25 dex) than in the VVDS (0.5 dex), however our error bars are compatible with the FDF result. This may suggest that our unsuccessful spectroscopic identification rate has a strong effect in our highest VVDS redshift bin, while our data points at $2.7 < z < 3.9$ appear fully consistent with the FDF.

8. The FUV luminosity densities at $0 < z < 5$

8.1. The global shape

Figure 9 displays the rest-frame FUV luminosity densities within the redshift range $0 < z < 5$. We find that the global luminosity density increases by a factor ~ 3.5 from $z = 0.05$ to $z = 1.2$, by a factor ~ 1.2 from $z = 1.2$ to $z = 3.4$, and decreases by a factor ~ 0.3 from $z = 3.4$ to $z = 5$. Furthermore the evolution at $1.1 < z < 3.0$ might be more complex than a modest increase. Indeed, even though our large error bars cannot exclude an increase or a plateau, our data points taken at face value exhibit a decrease

by a factor ~ 1.3 from $z = 1$ to $z = 2$, and an increase by a factor ~ 1.4 from $z = 2.0$ to $z = 3.4$. One could mention dust attenuation effects since at these redshifts, targets are selected from their rest-frame UV, and thus a fixed I -band flux cut could miss a non-negligible fraction of highly dust enshrouded targets. However, UV luminosity densities at $z \sim 3$ are larger than at $1 < z < 2$ while they should be even more dust affected since selected at shorter ultraviolet wavelengths.

The 1500 \AA luminosity density as a function of redshift from the FDF (Gabasch et al. 2004) presents a similar shape to that derived from the VVDS. We stress that both datasets, the FDF and the VVDS, span the redshift range $0.5 < z < 5$ within one single survey and have the same unique I -band selection criterion. We note that the FDF used photometric redshift techniques with NIR photometry, which gives reliable redshifts at $1 < z < 2$. The VVDS and the FDF are complementary; the VVDS is ~ 50 times larger in surface than the FDF and it consists of spectroscopic redshifts, while the FDF goes 2.8 mag deeper than the VVDS using photometric redshifts. Both estimates are in agreement, in particular at $1 < z < 2$.

We note that the empirical models from Pérez-González et al. (2005) also show a decrease in the cosmic SFR density

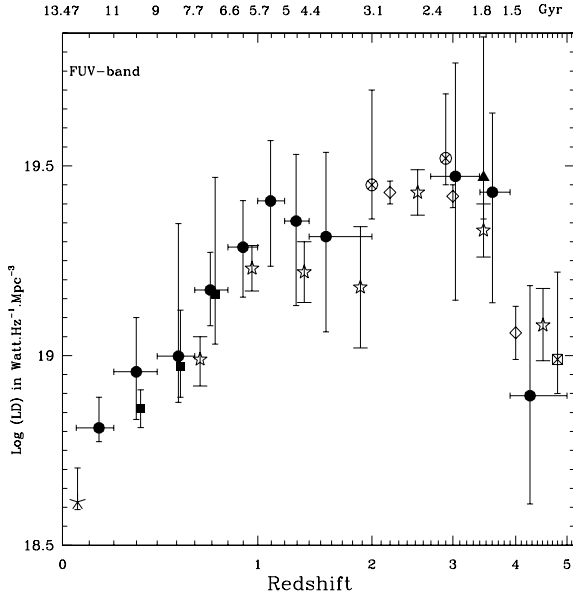


Fig. 9. Comoving non dust-corrected FUV luminosity densities from $z = 0$ to $z = 5$. The *plain circles* represent the 1500 \AA VVDS data ($0.05 < z < 5$) (see values and error bars in Tables 1 & 4), the *plain triangle* represents the 1500 \AA VVDS data at $3 < z < 4$ derived as in Paltani et al. (2007), and the *plain squares* represent the 1500 \AA GALEX-VVDS data at $z < 1$, plotted at $+0.02$ in redshift for clarity, from Schiminovich et al. (2005). Other data are the 1500 \AA GALEX-2dFGRS from Wyder et al. (2005) (asterisk), the 1500 \AA HDF data from Arnouts et al. (2005) (crossed circles), the 1700 \AA KDF data from Sawicki & Thompson (2006b) (open rhombus), the 1500 \AA FDF data from Gabasch et al. (2004) (open stars), and the 1700 \AA data from Iwata et al. (2007) (crossed square).

between $z = 1.4$ and $z = 2.2$, varying from 10 to 29 percent depending on the model but with luminosity evolution solely. It is interesting to see that their model including a combined luminosity plus number density evolution does not exhibit a decrease. Rather than excluding a number density evolution it indicates that the global emissivity is dominated by the luminosity evolution. We go into more detail about this effect in the next section.

We emphasize that our I -selected sample misses the very red ($I - K > 2.6$) galaxy population at $1.2 < z < 2.5$. This population concerns the most massive star forming dusty galaxies, as detailed in our K -selected sample described in Pozzetti et al. (2007).

8.2. The intrinsic luminosity dependency

The luminosity density is dominated by the evolution of the bright population. Thus we have integrated the LF from the three following absolute magnitude limits: $M_{AB}(1500 \text{ \AA}) < -19$ mag, $M_{AB}(1500 \text{ \AA}) < -20$ mag, and $M_{AB}(1500 \text{ \AA}) < -21$ mag. According to our LFs, these magnitude cutoffs correspond about to $L > L^*$ galaxies at $0.1 < z < 0.6$, $0.6 < z < 2$, and $2 < z < 3.4$ respectively. At $z \sim 0.05$, $M_{AB}^*(1500 \text{ \AA}) \sim -18$ mag (Wyder et al. 2005). We choose a fixed cutoff rather than a luminosity evolving cutoff to make a comparison over a long time baseline because this does not depend on the modeling of the luminosity evolution of the LF. The change of M^* with redshift implies that at $z \approx 3$ the most luminous galaxies were forming stars at a rate ~ 5 , and ~ 7 times higher than at $z \approx 0.15$, and $z \approx 0.05$ respectively. We have applied the same cutoffs to the LF

integration of the 1500 \AA HDF (Arnouts et al. 2005), the 1700 \AA KDF (Sawicki & Thompson 2006b), and the 1700 \AA data point of Steidel et al. (1999). Figure 10 displays these different luminosity densities for the bright population. We also produced the rest-frame FUV-band luminosity densities for three range of luminosities, $M_{AB}(1500 \text{ \AA}) > -19$ mag (dwarf and intermediate population, $< 0.1 L_{\text{Lyman Break Galaxy}}^*$), $-21 < M_{AB}(1500 \text{ \AA}) < -19$ (luminous population), and $M_{AB}(1500 \text{ \AA}) < -21$ (very luminous population, $> L_{\text{LBG}}^*$), as shown in Fig. 11.

8.2.1. Detailed results

We observe that on average the rest-frame FUV-band luminosity density of the ($2.7 < z < 5$) population is significantly brighter by a factor at least ~ 6 than the ($0.2 < z < 1.4$) population. This implies a transition phase for the population dominating the FUV emissivity. Another transition phase is observed at $z < 0.2$ with a steep decline by a factor of at least ~ 10 of the bright population luminosity density. Concentrating on the most luminous galaxies, and taking the values of \mathcal{L} at their face value, we can tentatively identify five phases from $z = 5$ to $z = 0$ as follows.

(a) From $z = 5$ to 3.4 , the emissivity due to galaxies brighter than $M_{AB}(1500 \text{ \AA}) < -20$ and -21 mag increases by a factor of ~ 3 and 2.5 respectively. The whole population, from the dwarf to the very luminous galaxies, sees its FUV luminosity increasing. This corresponds to a very active phase in terms of newly formed stars in every galaxy.

(b) From $z = 3.4$ to 1.4 , the emissivity due to galaxies brighter than $M_{AB}(1500 \text{ \AA}) < -20$ and -21 mag steadily decreases by a factor ~ 6 and 25 respectively. This ~ 3 Gyr phase corresponds to the progressive, but relatively quick, drop of star formation in the most luminous galaxies which are formed earlier than $z = 3.4$, and whose contribution to the global FUV luminosity density becomes less important toward lower redshifts. Lotz et al. (2006) observe that the distribution of the HST rest-frame FUV morphologies at $z \sim 1.5$ are similar to the ones at $z \sim 4$ with an identical fraction of major-merger candidates. This suggests that this drop is due to the same luminous galaxy population, and that it is not caused by a decrease in the number of mergers. Thus from $z = 3.4$, the most FUV luminous galaxy population has suddenly finished its stellar mass assembly and active star forming phase, while the less FUV luminous population is still very active and becomes the dominant star forming galaxy population until nowadays.

(c) From $z = 1.4$ to 0.6 , the emissivity due to galaxies brighter than $M_{AB}(1500 \text{ \AA}) < -20$ and -21 mag increases by a factor ~ 2 and 4 respectively. This corresponds to Fig. 2 in Zucca et al. (2006), where the fraction of the bright population (i.e. $L > L^*$) of early-type (E- and Sab-like) galaxies increases while the one for late-type (Scd-, Irr-like) galaxies decreases even though the latter still dominate in terms of numbers and also in emissivity (see Fig. 7) up to $z \sim 0.7$. This phase could correspond to merger events; indeed very disrupted HST morphologies in the very luminous galaxy population are generally observed. In the CDFS, we observe mergers within the early-type population as shown in Fig. 2 of Ilbert et al. (2006a) and also that the volume density of red, bright bulge-dominated galaxies increases by a factor ~ 2.7 from $z \sim 1$ to $z \sim 0.7$. Furthermore from $z = 1.5$ to $z = 0.6$ we find in Ilbert et al. (2006b) that rest-frame B -band \mathcal{L} for galaxies lying in over-dense environments (at a scale of $5h^{-1}$ Mpc) increases by a factor 1.2, while the one for those in under-dense environments continuously decreases by a factor of 2.3. Since the most luminous galaxies are usually

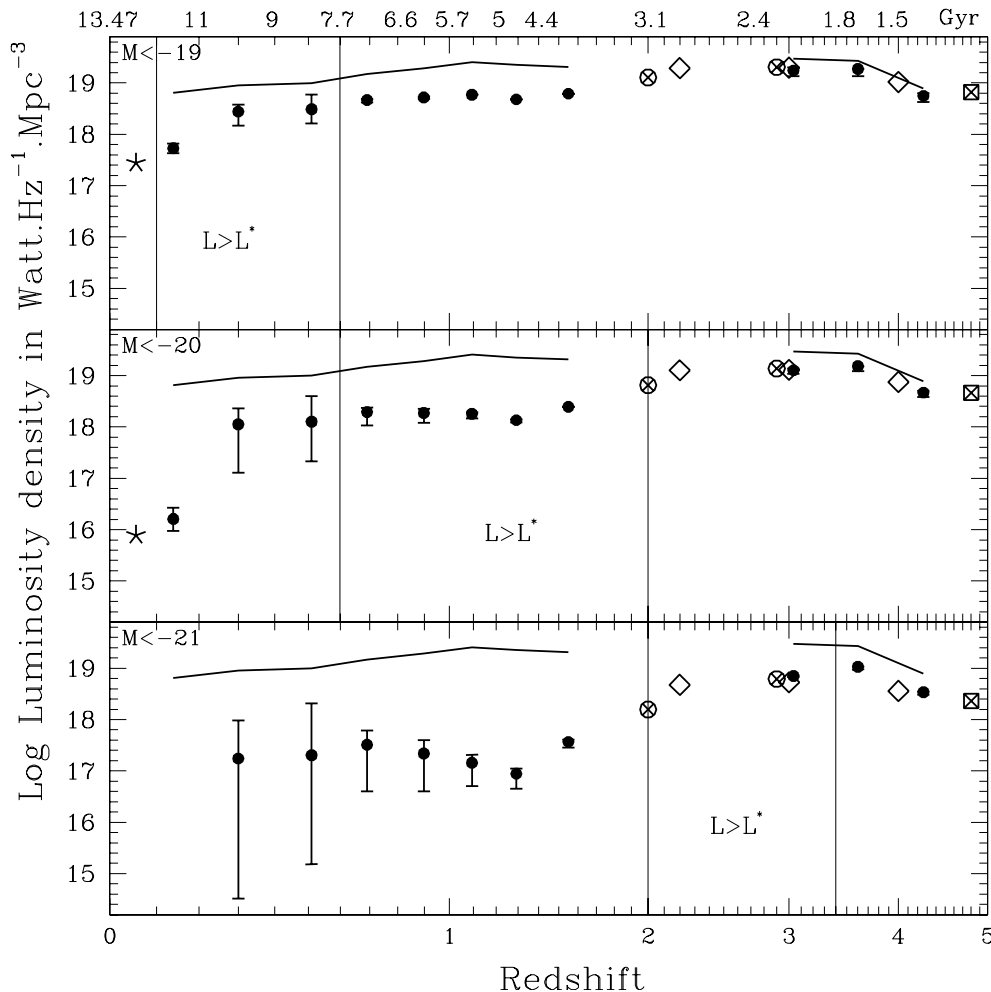


Fig. 10. Comoving rest-frame FUV non dust-corrected luminosity densities from $z = 0$ to $z = 5$ for three bright populations defined as $M_{AB}(1500 \text{ \AA}) < -19, -20,$ and -21 mag. Symbols are the same as in Fig. 9. Error bars correspond to the fixed slopes, $\alpha = -1.2$ and -1.75 at $0.2 < z < 5$, at $0.05 < z < 0.2$ to the fixed $M^* \pm 0.1$; those which are not visible are smaller than the size of the data point, i.e. < 0.1 dex. We do not plot the local values for $M < -21$ which have low values, at $z = 0.14$ and 0.055 $\text{Log } \mathcal{L} = 12.45 \pm 0.55$ and $12.10 \text{ Watt Hz}^{-1} \text{ Mpc}^{-3}$, respectively. In each panel, the solid line connects the VVDS points of the global FUV luminosity density as displayed in Fig. 9, and the vertical lines delimit the approximative redshift range in which the bright population is more luminous than the characteristic FUV luminosity of the whole population.

found in dense environments, our results favor the merging event to build-up early-type galaxies. The exact percentage of merger events is still hotly debated. We note also that it corresponds also to the phase where the less luminous population has reached its peak of star formation activity at $z \sim 1.1$. Another point is that at $1.5 < z < 2.5$, our I -selection is missing the reddest galaxies (Pozzetti et al. 2007), the dusty and massive sources as discovered in infrared surveys (i.e., e.g. Daddi 2004), and undergoing strong star forming and dusty phase. This population would be an excellent contributor to populate the FUV luminous population at $z < 1.4$ once the dusty phase linked to intense burst does not dominate anymore.

(d) From $z = 0.6$ to 0.2 , the emissivity due to galaxies brighter than $M_{AB}(1500 \text{ \AA}) < -20$ and -21 mag decreases by a factor ~ 1.3 and 1.5 respectively. The decrease of the bright part of the emissivity corresponds to a phase entirely dominated by the early-type galaxies for which the star formation decreases passively.

(e) From $z = 0.2$ to 0.05 , the emissivity due to galaxies brighter than $M_{AB}(1500 \text{ \AA}) < -20$ and -21 mag decreases by a factor ~ 100 and 25 respectively; the bright part of the

global FUV luminosity density abruptly drops. Analysing the $0 < z < 0.3$ CFRS spectra, Tresse et al. (1996) found that only 54 percent of galaxies exhibit strong star formation with $H\alpha$ and $H\beta$ both in emission and 15 percent have $H\alpha$ and $H\beta$ both in absorption. The remaining 31 percent is the intermediate population which shows spectral features from both star burst and quiescent stellar evolution. Therefore star formation seems to have slowed down or stopped in a significant fraction of galaxies in the nearby Universe. This population might correspond to the descendants of L^* galaxies at $0.2 < z < 1.4$ which when they fade in luminosity, stop dominating the rest-frame FUV-band luminosity densities. We note that the local sudden drop might be combined with the local underdensity seen in optical redshift surveys (Zucca et al. 1997; Tresse & Maddox 1998).

In resume, we observe a first major crisis for producing efficiently new stars, lasting ~ 3 Gyr, from $z \sim 4$ to $z \sim 1$, which involves the most massive and luminous galaxies ($M_{AB}(1500 \text{ \AA}) < -21$, $M_* > 10^{11} M_\odot$). While gradual fading of the global population starts at $z \sim 1$, we observe a second major crisis which started ~ 3 Gyr ago when star formation was progressively stopping in intermediate mass and luminosity galaxies

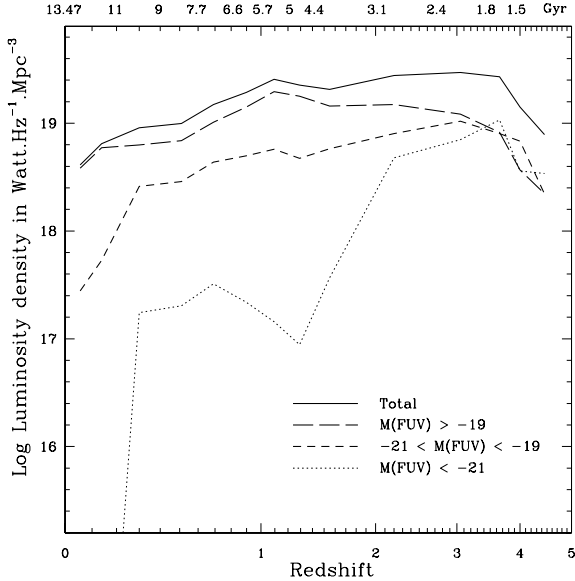


Fig. 11. Comoving rest-frame FUV non dust-corrected VVDS luminosity densities from $z = 0$ to $z = 5$ for three luminosity-class populations defined as $M_{AB}(1500 \text{ \AA}) > -19$ (dwarf and intermediate-luminosity galaxies, $< 0.1 L_{LBG}^*$), $-21 < M_{AB}(1500 \text{ \AA}) < -19$ (luminous galaxies), and $M_{AB}(1500 \text{ \AA}) < -21$ (very luminous galaxies, $> L_{LBG}^*$). We used and connected the same VVDS dataset as displayed in Fig. 10.

($-20 < M_{AB}(1500 \text{ \AA}) < -19$, $10^9 < M_* < 10^{11} M_\odot$). The period from $z = 1.4$ to $z = 0.6$ is highly intricate due to intertwining populations that follow different evolutionary path. Nevertheless the combined effects of decreasing both luminous and intermediate population is to make the global luminosity density decrease faster at $z < 1.2$ than at $1.2 < z < 3.9$.

8.2.2. Evolution of $L > L^*$ galaxies

According to the Schmidt law of star-forming galaxies (Kennicutt et al. 1998), the SFR is scaled to the cold gas density to the 1.4 power. Thus, once the gas reservoir is exhausted, star formation ceases. The old, most luminous and massive galaxies have exhausted their gas reservoir during their early intense star formation $z \geq 3.5$ (see previous section), and since then they undergo passive evolution as star formation ceases. This creates excellent dry candidates, that is cold gas-depleted to prevent new star formation.

Creation of new galaxies occurs as the threshold amplitude for forming bright galaxies decreases as described in Marinoni et al. (2005) from the VVDS data. That is, the typical L^* of the population created at a given z will decrease with decreasing redshift. This implies that younger, less massive and less luminous L^* galaxies continue to efficiently form stars with a large reservoir of cold gas at $0.2 < z < 3.9$. This intermediate galaxy population presents a peak of SFR at $z \sim 1$. And at $z < 0.2$ these galaxies appear to have also exhausted their gas as suggested by the 1500 \AA \mathcal{L} drop, and start to evolve passively. The gas-exhaustion would favor the evolution of morphologies toward early-type galaxies.

In resume, the global FUV luminosity density decreases faster at $z < 1.2$ than at $z < 3.9$ since it combines the decrease from both luminous and intermediate populations. During the phase $1.2 < z < 3.9$ it undergoes a decline of 0.06 dex, while for the phase $0.2 < z < 1.2$ it is 0.45 dex. The small decrease corresponds to the phase where the dwarf and intermediate

galaxy population increases its SFR, while the luminous population start to undergo its SFR decline. In Fig. 9, the global luminosity density might decrease by ~ 0.1 dex from $z = 3.9$ to $z \sim 2$, then increase by ~ 1.2 dex from $z \sim 2$ to $z = 1.2$. Nevertheless, our large error bars do not exclude a smooth decrease by 0.06 dex from $z = 3.9$ to $z = 1.2$.

At $z \lesssim 4$, both processes, i.e. dry mergers toward decreasing redshift and morphologies evolving toward early-type galaxies, might contribute to an increase of the bright early-type population by a factor ~ 10 to reach ~ 55 percent of the total population from $z = 1.5$ to $z = 0.2$, while the early-type population undergoes a passive luminosity evolution as shown by Zucca et al. (2006). It is in agreement with semi-analytical studies, e.g. Kaviraj et al. (2006) find that less than 50 percent of the stellar mass which ends up in early-types today is actually in early-type progenitors at $z \sim 1$, or De Lucia et al. (2006) find that 50 percent of local elliptical accrete half of their stellar mass out $z \sim 0.8$.

9. The history of the star formation rate density

We derive the SFR densities which are not dust corrected using the rest-frame 1500 \AA luminosity densities of the VVDS from $z = 0$ to $z = 5$. The SFR calibration of Madau et al. (1998) yields $SFR = 8 \times 10^{27} L(1500 \text{ \AA}/\text{erg s}^{-1} \text{ Hz}^{-1}) M_\odot \text{ yr}^{-1}$ for a Salpeter (1955)'s IMF including stars from 0.1 to 125 solar mass. We recall that at $0 < z < 1$, our 1500 \AA rest-frame band spans ultraviolet wavelengths shorter than 3000 \AA , that is a non-observed wavelength range with the optical bands. Nevertheless, we checked that our results are fully consistent with the rest-frame 1500 \AA GALEX-VVDS data (see details in Sect. 4.2). We present our SFR density in Fig. 12.

9.1. Dust obscuration

Our FUV data are not dust corrected. In the following, we compare them to data which account for dust at $z < 2.0$ to estimate the global correction needed to recover the total SFR density. That is, we use the $H\alpha$ nebular emission line dust-corrected data taken from Tresse et al. (2002), and the $12 \mu\text{m}$ mid-infrared continuum data from Pérez-González et al. (2005). These results are both described with an evolution proportional to $\sim (1+z)^4$, while the evolution of 1500 \AA \mathcal{L} in the VVDS is best described by $\sim (1+z)^2$ (see Sect. 4.1). Assuming an average dust correction for the whole field galaxy population, the dust obscuration at 1500 \AA is $\sim 1.8\text{--}2$ mag from $z = 2$ to $z = 0.4$. And from $z = 0.4$ to $z = 0$, it becomes smaller from ~ 2 down to $\sim 0.9\text{--}1$ mag.

The apparent dust transition at $z < 0.5$ corresponds exactly to the change of the dominant population as seen in Fig. 7 where the early-type galaxy B -band emissivity starts to dominate below $z = 0.4$. The early-type population is known to be dust deficient, and thus the needed amount of dust obscuration is less strong as redshift decreases. Our argument assumes that the increasing early-type dominant population in the B -band emissivity holds in the UV -band emissivity. From $z = 0.5$ to $z = 2$, the B -band emissivity is dominated by the late-type population, which form stars from gaseous nebulae, and thus is attenuated by a constant factor. From $z = 2$ to $z = 4$, the star-forming high-mass galaxies still dominate the emissivity, and thus we expect a constant dust attenuation of 2 mag. We note that near-infrared surveys miss the faint blue galaxies at $z < 1.2$, while they include the extremely red galaxies at $z > 1.2$ as shown in Pozzetti et al. (2007). Still the $12 \mu\text{m}$ data from Pérez-González et al. (2005) exhibit a similar shape than the FUV data, which reinforces the no evolution of

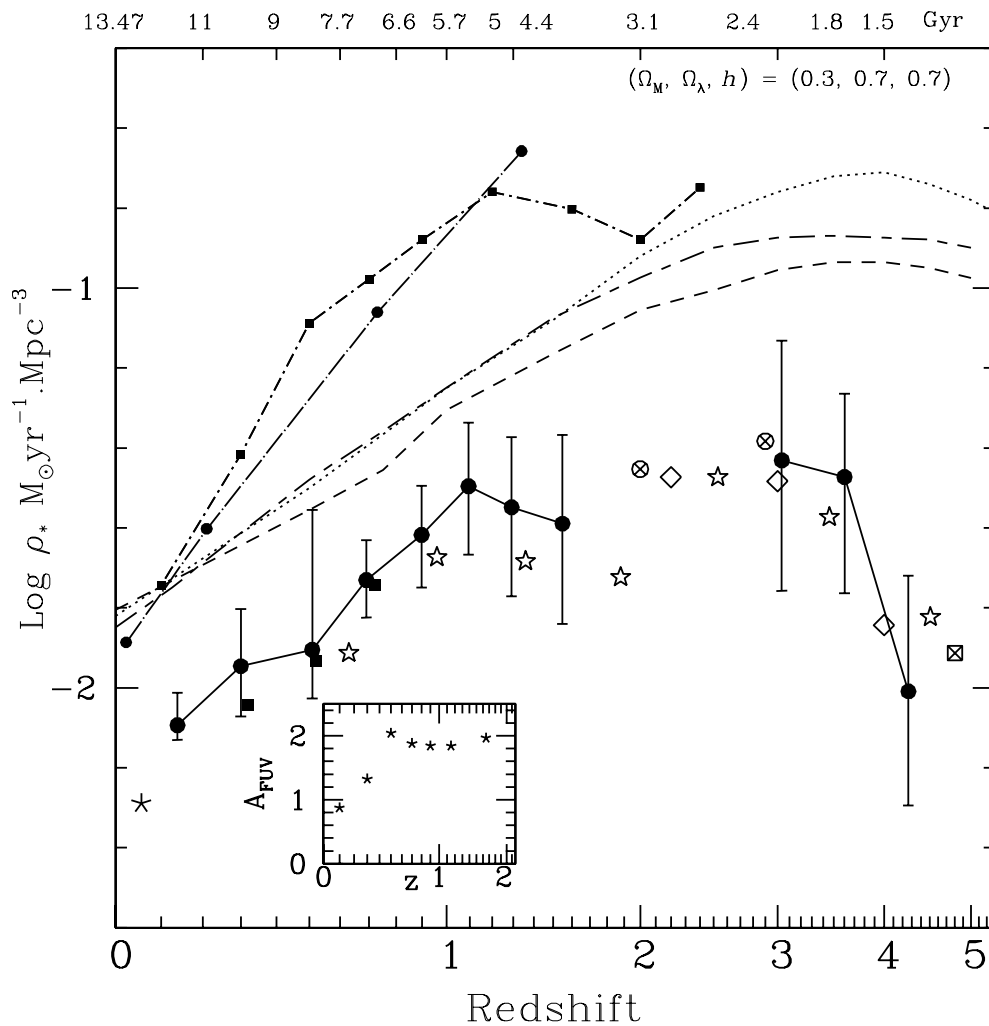


Fig. 12. Star formation rate densities as a function of redshift. Symbols (*plain large circles, plain large squares, asterisk, crossed circles, open rhombus, open stars, crossed square*) and error bars are the same as in Fig. 9, and they represent the SFR densities with no reddening correction. The dotted, long-dashed line connects the reddening corrected $H\alpha$ data (small plain circles) from the CFRS (Tresse & Maddox 1998; Tresse et al. 2002). The dotted, short-dashed line connects the $12\ \mu\text{m}$ data (small plain squares) from Pérez-González et al. (2005). Models from Somerville et al. (2001), Croton et al. (2006) and Nagamine et al. (2006) are represented with the dashed, the dotted, and the short-long dashed lines respectively. Everything is for a Salpeter (1955) IMF. The derived A_{FUV} dust obscuration between the VVDS data not dust corrected and the $12\ \mu\text{m}$ data at $z < 2$ is represented in the inset.

the dust content as shown by Bell et al. (2004) at $z < 1$ and Reddy et al. (2006) at $z > 1$. The dust correction might change again at $z > 4$ where the by-products of the physical processes to actively form star in massive galaxies will dominate through AGN and SN feedback.

We will make detailed dust obscuration estimates at $0 < z < 2$ in future papers using the VVDS-GALEX and -SWIRE data.

9.2. Comparison to simulations

In Fig. 12 we display the simulations from Somerville et al. (2001), Croton et al. (2006), and Nagamine et al. (2006). Comparing simulations with observational measurements might be severely affected by the assumed IMF, and the dust obscuration. These three simulations use the stellar population synthesis models of Bruzual & Charlot (1993). Nagamine et al. (2006) uses the IMF of Chabrier (2003), while the others use the one of Salpeter (1955). The SFR calibration of Nagamine et al. (2006) yields a conversion factor of 1.24×10^{28} for a Chabrier (2003) IMF including stars from 0.01 to 100 solar mass. It differs by

~ 0.2 in log from a Salpeter (1955) IMF, and thus, for consistency, we add this factor to the simulations of Nagamine et al. (2006). The dust prescription differs in a complex manner in each simulation. We do not attempt to homogenize the simulations in terms of dust obscuration.

The simulations all exhibit a peak of the SFR density at $z \sim 4$ with a smooth decrease up to $z = 0$. At a quick glance, they do not seem to go through the observational points, either dust corrected or not. However, at $2 < z < 3.9$, the simulations are close to our FUV data taken at face value if we assume a constant dust attenuation of ~ 2 mag as discussed in the previous paragraph. And, at $0 < z < 0.2$, the simulations are in good agreement with the dust corrected data ($H\alpha$ and $12\ \mu\text{m}$), or with FUV dust-corrected data by 1 mag. We note that Nagamine et al. (2006) used the dust extinction factors of Steidel et al. (1999), i.e. 1 mag for $z < 2$ and 1.7 mag for $z > 2$. Still, at $0.2 < z < 2$, the simulations do not reproduce the observational data. At $z < 0.2$ and $z > 2$, the global FUV emissivity is dominated by luminous, massive, large galaxies, while at $0.2 < z < 2$ it is dominated by the intermediate population.

10. Conclusions

We studied the first epoch VVDS data purely I -selected at [17.5–24] mag in (AB). The sample is unique in the sense that it goes deeper than previous I -selected spectroscopic samples, it has a well-defined selection function and it has enough data to study sub-samples. Within a single survey, we trace the evolution of the galaxy population dominating the total light at different redshifts all the way from $z = 5$ to $z = 0$. The main results of our comprehensive study are summarised below.

- i) To study the luminosity density evolution, observing deeper in flux is superior to assembling large samples as far as the galaxy sample is not dependent on cosmic variance and has a well-defined selection function. Nevertheless, the survey field must be large enough to identify the rare bright objects required to constrain the bright end of the LF.
- ii) The luminosity density evolution is substantially wavelength-dependent since the rest-frame passband luminosity is related more or less directly to very different stellar populations. We find that the non dust-corrected \mathcal{L} evolve with time over $0.05 \leq z \leq 1.2$, as $\mathcal{L} \propto (1+z)^x$ with $x = 2.05, 1.94, 1.92, 1.14, 0.73, 0.42$, and 0.30 in the FUV-1500, NUV-2800, U -3600, B -4400, V -5500, R -6500, and I -7900 passbands, respectively. Although error bars are still large, we note that most luminosity densities exhibit a transition at $z \approx 1.1$ in the evolutionary tendency. Over the last 8.5 Gyrs, the SFR-related FUV-band luminosity density drops by a factor 4. Recent merger events should produce little star formation.
- iii) The B -band luminosity density evolution is strongly type-dependent. From $z = 1.2$ to $z = 0.2$ the irregular-like, and Scd-like type galaxies decrease markedly by factors 3.5, and 1.7, respectively while the elliptical-like, and Sab-like types increase by factors 1.7, and 1.6, respectively. The late-type galaxy population undergoes a downsizing scenario where most star formation is shifting to intermediate- and low-mass galaxies at $z < 1.2$. The early-type galaxy population suggests a little contribution from merging or simple rest-frame color evolution phenomena, but it evolves passively in terms of luminosity, which suggests a very early formation stage ($z \gg 4$) for the majority of this red population.
- iv) The SFR density as seen in the rest-frame FUV-1500 luminosity density without dust correction undergoes the several following up-and-down phases as redshift decreases, and is strongly luminosity dependent. From $z = 5$ to $z = 3.4$, it increases by at most a factor ~ 3.5 , and it corresponds to the end of the mass assembly of the most luminous galaxies, $M_{AB}(1500 \text{ \AA}) < -21$ ($L > L_{LBG}^*$), which present a peak of SFR at $z \approx 3.5$. From $z = 3.4$ to $z = 1.2$ it decreases by a factor 1.2. Notwithstanding the large error bars this small decrease might be the result of two opposite processes; a decrease by a factor ~ 1.4 from $z = 3.4$ to $z = 2$ due to the fading of the giant galaxy population by a factor 40, and an increase by a factor ~ 1.3 from $z = 1.2$ to $z = 1.0$ due to the shift of the star formation activity towards the less luminous ($-21 < M_{AB}(1500 \text{ \AA}) < -19$) galaxy population which presents a peak of SFR at $z \sim 1$. From $z = 1.2$ to $z = 0.05$ it declines steadily by a factor 4, since this phase undergoes the fading of both the giant and the intermediate galaxy populations. Nevertheless it hides a strong SFR drop by a factor 100 at $z < 0.2$ of the intermediate galaxy population. This phenomena might be combined to the local underdensity seen in optical redshift surveys (see Zucca et al. 1997; Tresse & Maddox 1998), and thus the local Universe might not be an

excellent reference local point to trace back the evolution of the global galaxy population. Our observed global evolution does not seem to be in agreement with a continuous smooth decrease from $z \sim 2$ to $z \approx 0$ as predicted by the simulations.

- v) Comparing our SFR FUV-derived densities with mid-infrared or $H\alpha$ SFR-derived densities, we find that at $0.4 \lesssim z \lesssim 2$ the FUV is obscured by a constant factor of ~ 1.8 – 2 mag, and at $z < 0.5$ it is progressively less obscured down to ~ 0.9 – 1 mag. In parallel, we find that from $z = 0.4$ to $z = 0.05$ the B -band luminosity density is more and more dominated by the early-type (E/Sab-like) galaxy population which is known to be dust deficient. Further analysis combining VVDS-GALEX-SWIRE data will refine this result.
- vi) We conclude that the old, most luminous and massive galaxies have exhausted their cold gas reservoir during their early intense star formation which has occurred in the early Universe at $z \gg 4$, and since $z \approx 3.5$, i.e. ~ 12 Gyrs, they undergo passive evolution as star formation ceases. This creates excellent dry merger candidates, that is, in which gas has been sufficiently depleted that it prevents new star formation. The small level of contribution of dry-mergers remains to be quantified. Younger, less massive and less luminous L^* galaxies continue to efficiently form stars with a large reservoir of cold gas up to $z = 0.2$. And at $z < 0.2$ these galaxies appear to have also exhausted their gas supply as suggested by the FUV-band luminosity density noticeable drop, and start to evolve passively, and might be combined with a local underdensity. This picture is consistent with the downsizing scenario for the star formation (Cowie et al. 1996). We recall that the luminosity and SFR densities are mainly dominated by the $L^*\phi^*$ galaxies rather than the dwarf population which is usually undergoing density evolution (Ilbert et al. 2005). At $z < 3.5$ dry mergers and morphologies evolving towards early-type galaxies might contribute to increase the number density of the bright early-types in maintaining a passive luminosity evolution as observed by Zucca et al. (2006) at $0 < z < 1.5$, and also to increase the emissivity in over-dense regions as observed by Ilbert et al. (2006b).

Acknowledgements. This research was developed within the framework of the VVDS consortium. We thank the ESO staff at Paranal for their help in the acquisition of the data. We thank C. Moreau for her work on the VVDS database at LAM. This work was partially supported in France by the Institut National des Sciences de l'Univers of the Centre National de la Recherche Scientifique (CNRS), and its Programme National de Cosmologie and Programme National de Galaxies, and in Italy by the Ministry (MIUR) grants COFIN2000 (MM02037133) and COFIN2003 (num. 2003020150). The VLT-VIMOS observations were carried out on guaranteed time (GTO) allocated by the European Southern Observatory (ESO) to the VIRMOS consortium under a contractual agreement between the CNRS, heading a consortium of French and Italian institutes, and ESO to design, manufacture and test the VIMOS instrument.

References

- Arnouts, S., Schiminovich, D., Ilbert, O., et al. 2005, ApJ, 619, L43
 Baldry, I. K., Glazebrook, K., Budavári, T., et al. 2005, MNRAS, 358, 441
 Bell, E., Wolf, C., Meisenheiner, K., et al. 2004, ApJ, 608, 752
 Blanton, M. R., Hogg, D. W., Bahcall, N., et al. 2003, ApJ, 592, 819
 Bottini, D., Garilli, B., Maccagni, D., et al. 2005, PASP, 117, 996
 Bruzual, A. G., & Charlot, S. 1993, ApJ, 405, 538
 Coleman, G. D., Wu, C.-C., & Weedman, D. W. 1980, ApJS, 43, 393
 Cowie, L. L., Songalia, A., Hu, E. M., & Cohen, J. G. 1996, AJ, 112, 839
 Croton, D., Springel, V., White, S. D. M. et al. 2006, MNRAS, 365, 11
 Chabrier, G. 2003, ApJ, 586, L133
 Daddi, E., Cimatti, A., Renzini, A., et al. 2004, ApJ, 600, L127
 de Lapparent, V. 2003, A&A, 408, 845
 de Lucia, G., Springel, V., White, S. D. M., et al. 2006, MNRAS, 366, 499

- Faber, S., Willmer, C. N. A., Wolf, C., et al. 2005, *ApJ*, submitted
[arXiv:astro-ph/0506044]
- Feulner, G., Bender, R., Drory, N., Hop, U., Snigula, J., & Hill, G. J. 2003, *MNRAS*, 342, 605
- Fioc, M., & Rocca-Volmerange, B. 1997, *A&A*, 326, 950
- Fontana, A., Pozzetti, L., Donnarumma, I., et al. 2004, *A&A*, 424, 23
- Franzetti, P., Scodreggio, M., Garilli, B., et al. 2007, *A&A*, 465, 711
- Gabasch, A., Bender, R., Seitz, S., et al. 2004, *A&A*, 421, 41
- Gallego, J., Zamorano, J., Aragon-Salamanca, A., & Rego, M. 1995, *ApJ*, L1
- Hopkins, A. M. 2004, *ApJ*, 615, 209
- Hopkins, A. M., & Beacom, J. F. 2006, *ApJ*, 651, 142
- Ilbert, O., Tresse, L., Arnouts, S., et al. 2004, *MNRAS*, 351, 541
- Ilbert, O., Tresse, L., Zucca, E., et al. 2005, *A&A*, 439, 863
- Ilbert, O., Lauger, S., Tresse, L., et al. 2006a, *A&A*, 453, 809
- Ilbert, O., Cucciati, O., Marinoni, C., et al. 2006b, *A&A*, submitted
[arXiv:astro-ph/0602329]
- Ilbert, O., Arnouts, S., McCracken, H. J., et al. 2006c, *A&A*, 457, 841
- Iwata, I., Ohta, K., Tamura, N., et al. 2007, *MNRAS*, 376, 1557
- Kaviraj, S., Devriendt, J. E. G., Ferreras, I., Yi, S. K., & Silk, J. 2006, *MNRAS*, submitted [arXiv:astro-ph/0602347]
- Kennicutt, R. C. ApJ, 498, 541
- Le Fèvre, O., Crampton, D., Lilly, S. J., Hammer, F., & Tresse, L. 1995, *ApJ*, 455, 60
- Le Fèvre, O., Saisse, M., Mancini, D., et al. 2003, *SPIE*, 4841, 1670
- Le Fèvre, O., Mellier, Y., McCracken, H. J., et al. 2004a *A&A*, 417, 839
- Le Fèvre, O., Vettolani, G., Paltani, S., Tresse, L., et al. 2004b, *A&A*, 428, 1043
- Le Fèvre, O., Vettolani, G., Garilli, B., Tresse, L., et al. 2005a, *A&A*, 439, 845
- Le Fèvre, O., Paltani, S., Arnouts, S., et al. 2005b, *Nature*, 437, 519
- Lilly, S. J., Tresse, L., Hammer, F., Crampton, D., & Le Fèvre, O. 1995, *ApJ*, 455, 108
- Lilly, S. J., Le Fèvre, O., Hammer, F., & Crampton, D. 1996, *ApJ*, 460, 1
- Loveday, J., Peterson, B. A., Efstathiou, G., & Maddox, S. J. 1992, *ApJ*, 390, 338
- Lotz, J., Madau, P., Giavalisco, M., Primack, J., & Ferguson, H. C. 2006, *ApJ*, 636, 592
- Madau, P., Ferguson, H. C., Dickinson, M. E., et al. 1996, *MNRAS*, 283, 1388
- Madau, P., Pozzetti, L., & Dickinson, M. 1998, *ApJ*, 498, 106
- Marinoni, C., Le Fèvre, O., Meneux, B., et al. 2005, *A&A*, 442, 801
- Martin, D. C., Fanson, J., Schiminovich, D., et al. 2005, *ApJ*, 619, L1
- Nagamine, K., Ostriker, J. P., Fukugita, M., & Cen, R. 2006, *ApJ*, 653, 881
- Norberg, P., Cole, S., Baugh, C., et al. 2002, *MNRAS*, 336, 907
- Oke J. B. 1974, *ApJS*, 236, 27
- Paltani, S., Le Fèvre, O., Ilbert, O., et al. 2007, *A&A*, 463, 873
- Pérez-González, P. G., Pablo, G., Rieke, G. H., et al. 2005, *ApJ*, 630, 82
- Poli, F., Giallongo, E., Fontana, A., et al. 2003, *ApJ*, 593, L1
- Pozzetti, L., Bolzonella, M., Lamareille, F., et al. 2007, *A&A*, in preparation
- Reddy, N. A., Steidel, C. C., Fadda, D., et al. 2006, *ApJ*, 644, 792
- Salpeter, E. E. 1955, *ApJ*, 121, 161
- Sandage, A., Tammann, G. A., Yahil, A. 1979, *ApJ*, 232, 352
- Sawicki, M., & Thompson, D. 2006a, *ApJ*, 642, 653
- Sawicki, M., & Thompson, D. 2006b, *ApJ*, 648, 299
- Shechter, P. 1976, *ApJ*, 203, 297
- Schiminovich, D., Ilbert, O., Arnouts, S., et al. 2005, *ApJ*, 619, L47
- Scodreggio, M., Franzetti, P., Garilli, B., et al. 2005, *PASP*, 117, 1284
- Somerville, R. S., Primack, J. R., & Faber, S. M. 2001, *MNRAS*, 320, 504
- Steidel, C. C., Giavalisco, M., Pettini, M., Dickinson, M., & Adelberger, K. L. 1996, *ApJ*, 462, L17
- Steidel, C. C., Adelberger, K. L., Giavalisco, M., Dickinson, M., & Pettini, M., 1999, *ApJ*, 519, 1
- Tresse, L., Rola, C., Hammer, F., et al. 1996, *MNRAS*, 281, 847
- Tresse, L., Maddox, S. J., Le Fèvre, O., & Cuby, J.-G. 2002, *MNRAS*, 337, 369
- Tresse, L., & Maddox, S. J. 1998, *ApJ*, 495, 691
- Zucca, E., Zamorani, G., Vettolani, G., et al. 1997, *A&A*, 326, 477
- Zucca, E., Ilbert, O., Bardelli, A., et al. 2006, *A&A*, 455, 879
- Wilson, G., Cowie, L. L., Barger, A. J., Burke D. J. 2002, *AJ*, 124, 1258
- Wyder, T., Treyer, M., Milliard, B., et al. 2005, *ApJ*, 619, L11

¹ Laboratoire d'Astrophysique de Marseille (UMR 6110), CNRS-Université de Provence, BP 8, 13376 Marseille Cedex 12, France
e-mail: Laurence.Tresse@oamp.fr

² Institute for Astronomy, 2680 Woodlawn Dr., University of Hawaii, Honolulu, Hawaii 96822, USA

³ INAF-Osservatorio Astronomico di Bologna, via Ranzani 1, 40127 Bologna, Italy

⁴ Integral Science Data Centre, Ch. d'Écogia 16, 1290 Versoix, Switzerland

⁵ Geneva Observatory, Ch. de Maillettes 51, 1290 Sauverny, Switzerland

⁶ INAF-IASF, via Bassini 15, 20133 Milano, Italy

⁷ Laboratoire d'Astrophysique de l'Observatoire Midi-Pyrénées (UMR 5572), CNRS-Université Paul Sabatier, 14 avenue E. Belin, 31400 Toulouse, France

⁸ INAF-IRA, via Gobetti 101, 40129 Bologna, Italy

⁹ INAF-Osservatorio Astronomico di Roma, via di Frascati 33, 00040 Monte Porzio Catone, Italy

¹⁰ INAF-Osservatorio Astronomico di Capodimonte, via Moiariello 16, 80131 Napoli, Italy

¹¹ Institut d'Astrophysique de Paris (UMR 7095), 98bis boulevard Arago, 75014 Paris, France

¹² School of Physics & Astronomy, University of Nottingham, University Park, Nottingham NG72RD, UK

¹³ Astrophysical Institute Potsdam, An der Sternwarte 16, 14482 Potsdam, Germany

¹⁴ INAF-Osservatorio Astronomico di Brera, via Brera 28, 20121 Milano, Italy

¹⁵ Observatoire de Paris-LERMA, 61 avenue de l'Observatoire, 75014 Paris, France

¹⁶ Università di Bologna, Dipartimento di Astronomia, via Ranzani 1, 40127 Bologna, Italy

¹⁷ Centre de Physique Théorique (UMR 6207), CNRS-Université de Provence, 13288 Marseille, France

¹⁸ Astronomical Observatory of the Jagiellonian University, ul Orła 171, 30-244 Kraków, Poland

¹⁹ Università di Milano-Bicocca, Dipartimento di Fisica, Piazza delle Scienze 3, 2016 Milano, Italy